

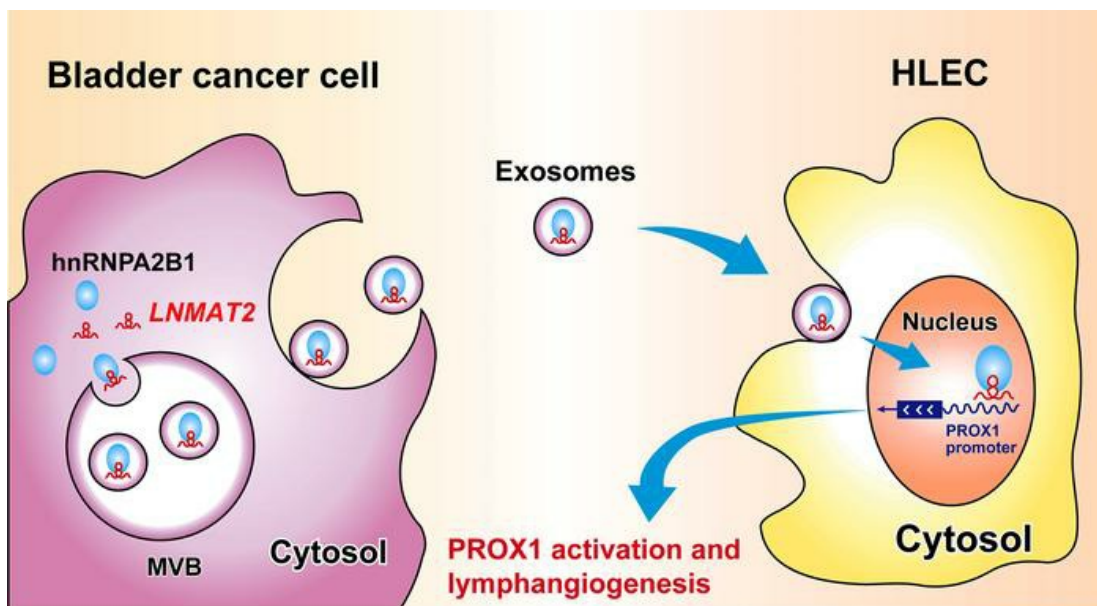
Exosomal long noncoding RNA *LNMAT2* promotes lymphatic metastasis in bladder cancer

Changhao Chen, ... , Rufu Chen, Tianxin Lin

J Clin Invest. 2019. <https://doi.org/10.1172/JCI130892>.

Research In-Press Preview Oncology

Graphical abstract



Find the latest version:

<https://jci.me/130892/pdf>



1 **Abstract**

2 Patients with bladder cancer (BCa) with clinical lymph node (LN) metastasis have
3 extremely poor prognosis. VEGF-C has been demonstrated to play vital roles in LN
4 metastasis in BCa. However, approximately 20% of BCa with LN metastasis exhibits low
5 VEGF-C expression, suggesting a VEGF-C-independent mechanism for LN metastasis of
6 BCa. Herein, we demonstrated that BCa cell-secreted exosomes-mediated lymphangiogenesis
7 promoted LN metastasis in BCa, which was in a VEGF-C-independent manner. We identified
8 an exosomal long noncoding RNA (lncRNA), termed lymph node metastasis-associated
9 transcript 2 (*LNMAT2*), stimulated HLEC tube formation and migration in vitro and enhanced
10 tumor lymphangiogenesis and LN metastasis in vivo. Mechanistically, *LNMAT2* was loaded
11 to BCa cell-secreted exosomes by directly interacting with heterogeneous nuclear
12 ribonucleoprotein A2B1 (hnRNPA2B1). Subsequently, exosomal *LNMAT2* was internalized
13 by HLECs and epigenetically upregulated prospero homeobox 1 (*PROX1*) expression by
14 recruitment of hnRNPA2B1 and increasing the H3K4 trimethylation level in the *PROX1*
15 promoter, ultimately resulting in lymphangiogenesis and lymphatic metastasis. Therefore, our
16 findings highlight a VEGF-C-independent mechanism of exosomal lncRNA-mediated LN
17 metastasis and identify *LNMAT2* as a therapeutic target for LN metastasis in BCa.
18

1 **Introduction**

2 Bladder cancer (BCa), one of the most commonly diagnosed malignancies worldwide, is
3 the leading cause of cancer-related death among men, with an estimated 550,000 new cases
4 and 20,000 deaths in 2018 (1). The prognosis of patients with BCa is closely associated with
5 the presence of lymph node (LN) metastasis, which decreases the 5-year survival rate from
6 77.6% to 18.6% (2). Despite the overwhelming evidence for the role of LN metastasis in
7 cancer, the definite molecular mechanism that triggers it in BCa remains unclear. We have
8 previously demonstrated that VEGF-C produced by tumor cells (3) and tumor-associated
9 macrophages (TAMs) (4) plays a crucial role in BCa lymphangiogenesis and LN metastasis.
10 However, approximately 20% of BCa with LN metastasis has low VEGF-C expression (5, 6),
11 which suggests the existence of a VEGF-C-independent mechanism for lymphangiogenesis
12 and LN metastasis in BCa.

13 Prospero homeobox 1 (PROX1) is essential for lymphatic vascular system formation,
14 regulating endothelial cell differentiation and inducing the lymphatic budding and extension
15 of lymphatic endothelial cells (7, 8). *Prox1*^{-/-} mice lack a lymphatic vascular system and die
16 within a few days after birth (9). PROX1 enhanced lymphatic endothelial cell proliferation
17 through synergistic interaction with p50 to activate VEGFR3 expression (10). Nevertheless,
18 the precise mechanism of cancer cell promotion of lymphangiogenesis and PROX1
19 upregulation remains unclear.

20 Exosomes are small microvesicles ranging 30-150 nm in size that contain various types of
21 nucleic acids, including mRNAs, miRNAs, and long noncoding RNAs (lncRNAs) (11, 12).
22 Recently, cancer cell-secreted exosomes were identified as crucial messengers in intercellular
23 communication associated with cancer-induced vascular permeability (13), inflammation (14),
24 and bone marrow progenitor cell recruitment in distant organs (15). For example,
25 EGFR-containing exosomes regulate the liver microenvironment to promote liver metastasis

1 (16), exosomal *miR-25-3p* participates in pre-metastatic niche formation (17), and exosomal
2 *miR-1247-3p* facilitates lung metastasis by activating cancer-associated fibroblasts (18).
3 However, the mechanism of cancer cell-secreted exosome regulation of lymphatic vascular
4 system formation via the induction of lymphangiogenesis remains unknown, warranting
5 further exploration.

6 Herein, we reported that an lncRNA, *LINC00858*, termed lymph node
7 metastasis-associated transcript 2 (*LNMAT2*), was overexpressed in BCa tissues and highly
8 enriched in urinary exosomes (urinary-EXO) from patients with BCa, and correlated
9 positively with LN metastasis. Exosomal *LNMAT2* promoted lymphangiogenesis and LN
10 metastasis in vitro and in vivo. Mechanistically, *LNMAT2* was loaded to exosomes by direct
11 interaction with heterogeneous nuclear ribonucleoprotein A2B1 (hnRNPA2B1) and
12 transmitted to human lymphatic endothelial cells (HLECs). Subsequently, *LNMAT2* formed a
13 triplex with the *PROX1* promoter and enhanced *PROX1* transcription by inducing
14 hnRNPA2B1-mediated H3 lysine 4 trimethylation (H3K4me3), facilitating
15 lymphangiogenesis and LN metastasis in BCa. Our findings highlight a
16 VEGF-C-independent mechanism of exosomal *LNMAT2*-mediated LN metastasis and
17 identify *LNMAT2* as a potential diagnostic marker and therapeutic target for LN metastasis in
18 BCa.

19

1 **Results**

2 ***LNMAT2 overexpression correlated with BCa LN metastasis***

3 Using next-generation sequencing (NGS), we previously explored the global expression
4 profiles of lncRNAs in high-grade muscle-invasive bladder cancer (MIBC) tissues and paired
5 normal adjacent tissues (NATs) from five patients with BCa and in five paired LN-positive
6 and LN-negative BCa tissues (4) (Gene Expression Omnibus ID: GSE106534). Statistical
7 analysis revealed that *LNMAT2* expression was increased by > 3-fold in the MIBC tissues
8 compared with the NATs and in the LN-positive BCa tissues compared with the LN-negative
9 tissues. Quantitative real-time PCR (qRT-PCR) confirmed *LNMAT2* overexpression in BCa
10 tissues from 266 patients compared with the corresponding NATs (Supplemental Figure 1A).
11 In humans, *LNMAT2* is located on chromosome 10q23.1 (RefSeq accession number:
12 MK692948, Supplemental Figure 1B), and the full-length 3187 nt *LNMAT2* in BCa cells was
13 determined by 5' and 3' rapid amplification of cDNA ends (RACE) assays (Supplemental
14 Figure 1, C-F). Fluorescence in situ hybridization (FISH) and subcellular fractionation assays
15 showed that *LNMAT2* mainly localized to BCa cell cytoplasm (Supplemental Figure 2, A-D).
16 Consistently, analyses of The Cancer Genome Atlas (TCGA) database showed that *LNMAT2*
17 was upregulated in multiple human cancers, such as BCa, uterine corpus endometrial cancer,
18 lung cancer, liver cancer, and stomach cancer (Supplemental Figure 3, A-F).

19 Moreover, a positive correlation was found between *LNMAT2* expression and LN
20 metastasis in a cohort of 266 BCa patients (Figure 1A and Supplemental Table 1). qRT-PCR
21 detected higher *LNMAT2* expression in metastatic tumor cells in the LNs than in BCa primary
22 tumors, suggesting that *LNMAT2* might contribute to BCa metastasis (Supplemental Figure
23 4A). Furthermore, Kaplan-Meier analysis revealed that *LNMAT2* overexpression correlated
24 with shorter overall survival (OS) and disease-free survival (DFS) in BCa patients (Figure 1,
25 B and C). Univariate and multivariate Cox analysis confirmed that *LNMAT2* expression

1 correlated independently with OS and DFS in BCa patients (Supplemental Table 2 and 3).
2 Consistently, the TCGA database results indicated a positive association between *LNMAT2*
3 overexpression and poor prognosis in human cancer, including lung cancer and stomach
4 cancer (Supplemental Figure 4, B-D). It is worth noting that *LNMAT2* overexpression was
5 highly correlated with reduced OS and DFS in LN-positive BCa patients (Supplemental
6 Figure 4, E and F). *LNMAT2* expression was significantly upregulated in the LN-positive
7 BCa tissues, slightly increased in LN-negative BCa tissues, and was rarely detected in NATs
8 by in situ hybridization (ISH) assay (Figure 1, D and E and Supplemental Figure 4G).
9 Importantly, *LNMAT2* expression was also positively correlated with lymphatic vessel density,
10 as indicated by the specific lymphatic vessel marker lymphatic vessel endothelial hyaluronan
11 receptor 1 (LYVE-1), but no correlation was observed between *LNMAT2* and VEGF-C
12 expression in BCa (Figure 1, F-H). Collectively, these results indicate that *LNMAT2*
13 overexpression-induced LN metastasis of BCa might be independent of VEGF-C.

14 ***LNMAT2 was enriched in BCa cell-secreted exosomes***

15 Prominently, ISH showed high *LNMAT2* expression in the extracellular space of BCa
16 (Figure 1D). We also found significantly higher extracellular *LNMAT2* expression in BCa
17 tissues with LN metastasis compared with BCa tissues without LN metastasis (Figure 1, D
18 and E), suggesting that extracellular *LNMAT2* might play a crucial role in BCa LN metastasis.
19 As extracellular lncRNAs are mainly encapsulated in specific subcellular materials,
20 exosomes in particular, and have important biological functions in mediating cell-cell
21 interactions and contributing to tumor LN metastasis (19), we then examined *LNMAT2*
22 expression in BCa cell-secreted exosomes. We used qRT-PCR to analyze the exosomes
23 isolated from the urine samples of 206 patients with BCa and 120 healthy controls and found
24 that *LNMAT2* was upregulated in the urinary-EXO obtained from BCa patients compared
25 with the healthy controls (Figure 2A), suggesting that exosomal *LNMAT2* is essential to the

1 development of BCa.

2 We further examined *LNMAT2* expression in exosomes isolated from the culture medium
3 of BCa cell lines (5637 and UM-UC-3). Exosomes with a typical cup-shaped morphology
4 and 30-150 nm in size were detected by transmission electron microscopy (TEM) (Figure 2B
5 and Supplemental Figure 4H) and NanoSight analysis (Figure 2C and Supplemental Figure
6 4I). Western Blot detection of the exosomal protein markers CD9 and CD63 confirmed that
7 the particles isolated from the culture medium were exosomes (Figure 2D and Supplemental
8 Figure 4J). *LNMAT2* expression was significantly upregulated in both the 5637 and
9 UM-UC-3 cells and their corresponding exosomes as compared with that in human normal
10 bladder epithelial cells (SV-HUC-1) (Figure 2E). Interestingly, *LNMAT2* enrichment was
11 detected in BCa cell-secreted exosomes relative to its expression in the cells, suggesting that
12 *LNMAT2* may exert its main function in exosomal form (Figure 2E). *LNMAT2*
13 overexpression via *LNMAT2* plasmid transfection led to an obvious increase of *LNMAT2*
14 levels in the BCa cell-secreted exosomes (Figure 2, F and G), while silencing *LNMAT2* had
15 the opposite effect (Figure 2, H and I), suggesting that altering cellular *LNMAT2* expression
16 significantly impacts exosomal *LNMAT2* expression, solidifying our hypothesis that
17 extracellular *LNMAT2* exists mainly in exosomal form. Taken together, our results indicate
18 that *LNMAT2* is abundant in BCa cell-secreted exosomes.

19 ***BCa cell-secreted exosomal LNMAT2 promoted lymphangiogenesis in vitro***

20 Since lymphangiogenesis is the rate-determining step for LN metastasis in BCa (20), we
21 then investigated whether upregulating *LNMAT2* expression could facilitate
22 lymphangiogenesis in vitro. The tube formation and migration in HLECs incubated with BCa
23 cell-secreted exosomes were analyzed. The BCa cells-secreted exosomes dramatically
24 promoted HLEC tube formation and migration as compared with the control (Figure 3, A-C).
25 Moreover, the exosomes secreted by *LNMAT2*-overexpressing UM-UC-3 cells

1 (UM-UC-3-EXO_{LNMAT2}) strongly induced HLEC tube formation and migration (Figure 3,
2 D-F). Conversely, exosomes secreted by *LNMAT2*-silenced 5637 cells (5637-EXO_{si-LNMAT2})
3 lost the ability to induce HLEC tube formation and migration (Figure 3, G-I). These results
4 indicate that exosomal *LNMAT2* contributes to lymphangiogenesis in vitro.

5 ***Exosomal LNMAT2 promoted lymphatic metastasis in vivo***

6 Although we observed that *LNMAT2* knockdown led to reduced and *LNMAT2*
7 overexpression led to an increase in the growth rates of BCa cells, as indicated by CCK-8,
8 colony formation and EdU assays (Supplemental Figure 5, A-H), dysregulation of *LNMAT2*
9 has no obvious effect on the invasiveness of BCa cells, which provided further evidence that
10 exosomal *LNMAT2* plays vital roles in LN metastasis.

11 To further examine the effect of exosomal *LNMAT2* on LN metastasis, we established a
12 popliteal lymphatic metastasis model using similar modeling approaches as described
13 previously (4, 21). Luciferase-labeled UM-UC-3 cells were implanted in the footpads of nude
14 mice, which were then randomly divided into three groups ($n = 12$), followed by intratumoral
15 injection with PBS (control), exosomes secreted by vector-transfected UM-UC-3 cells
16 (UM-UC-3-EXO_{vector}), or exosomes secreted by *LNMAT2*-transfected UM-UC-3 cells
17 (UM-UC-3-EXO_{LNMAT2}) every 3 days. When the primary tumor reached 200 mm³, the tumors
18 and popliteal LNs were excised (Figure 4A). Interestingly, IVIS live in vivo imaging system
19 showed that UM-UC-3-EXO_{LNMAT2} significantly promoted the ability of BCa cells to
20 metastasize to the LNs as compared with the control or UM-UC-3-EXO_{vector} groups (Figure 4,
21 B and C). The volume of popliteal LNs in the UM-UC-3-EXO_{LNMAT2} group were significantly
22 larger than that in the control or UM-UC-3-EXO_{vector} groups (Figure 4, D and E). Luciferase
23 immunostaining indicated increased metastatic LNs in the UM-UC-3-EXO_{LNMAT2} group,
24 which confirmed that exosomal *LNMAT2* significantly enhanced the metastatic capability of
25 BCa cells to LNs (Figure 4, F and G and Supplemental Table 4). Taken together, these results

1 suggest that exosomal *LNMAT2* plays an important part in LN metastasis of BCa in vivo.

2 Tumorigenicity is a major factor underlying lymphangiogenesis and LN metastasis (22),
3 and is closely associated with LN involvement in various solid tumors, such as lung cancer
4 (23), gastric cancer (24), and appendix neuroendocrine tumor (25). Therefore, we
5 investigated the tumorigenic capacity of exosomal *LNMAT2* in vivo using a subcutaneous
6 xenograft model as previously reported (3, 21). Mice were inoculated subcutaneously with
7 UM-UC-3 cells and randomly separated into three groups ($n = 12$). Each group received
8 intratumoral PBS, UM-UC-3-EXO_{vector}, or UM-UC-3-EXO_{*LNMAT2*} every 3 days for 5
9 consecutive weeks (Figure 5A). UM-UC-3-EXO_{*LNMAT2*} enhanced tumor growth compared
10 with both UM-UC-3-EXO_{vector} group and the control group (Figure 5, B-D). Tumors in
11 UM-UC-3-EXO_{*LNMAT2*} group were of greater size and weight (Figure 5, E and F) and had
12 higher expression levels of the proliferation marker Ki67 as compared with the
13 UM-UC-3-EXO_{vector} and control groups (Figure 5, G and H). Collectively, these results
14 indicate that BCa cell-secreted exosomal *LNMAT2* can promote lymphangiogenesis and LN
15 metastasis in vivo.

16 ***LNMAT2 interacted directly with hnRNPA2B1***

17 Next, we investigated the molecular mechanism and interacting partners of *LNMAT2* in
18 BCa. In vitro RNA pull-down assays with biotinylated *LNMAT2* and antisense control
19 showed an obvious 35-40 kDa band (Figure 6A), which mass spectrometry (MS) confirmed
20 was hnRNPA2B1 (Figure 6B). Western Blot analysis of *LNMAT2*-enriched proteins after
21 RNA pull-down indicated that *LNMAT2* bound specifically to hnRNPA2B1 (Figure 6, C and
22 D). Consistently, confocal microscopy of *LNMAT2* FISH and hnRNPA2B1 immunostaining
23 showed that *LNMAT2* and hnRNPA2B1 colocalized mostly in the cytoplasm of BCa cells
24 (Figure 6E). RNA immunoprecipitation (RIP) showed enrichment of *LNMAT2* by
25 hnRNPA2B1, validating the interaction between *LNMAT2* and hnRNPA2B1 (Figure 6F and

1 Supplemental Figure 6A). Moreover, serial deletion analysis determined that the 1900-2100
2 nt region of *LNMAT2* was indispensable for direct interaction with hnRNPA2B1 (Figure 6, G
3 and H). hnRNPA2B1, an RNA-binding protein (RBP), is involved in cytoplasmic RNA
4 trafficking through the recognition of specific sequences on the target RNA (26). Sequence
5 analysis by POSTAR2 (27, 28) indicated a sequence motif and structural preference of the
6 RBP binding site for hnRNPA2B1 (Figure 6I), which was located in the 1930-1960 nt region
7 of *LNMAT2* and formed a stem-loop structure (Figure 6J). RIP performed after site-directed
8 mutagenesis of this region revealed that it was critical to *LNMAT2* interaction with
9 hnRNPA2B1 (Figure 6K and Supplemental Figure 6B).

10 ***hnRNPA2B1 mediated LNMAT2 packaging into exosomes***

11 RNAs are selectively loaded into exosomes by RBPs (29, 30), including hnRNPA2B1.
12 Accordingly, we examined whether the direct interaction of *LNMAT2* with hnRNPA2B1
13 contributed to the packaging of *LNMAT2* into exosomes. As shown in Figure 7A and
14 Supplemental Figure 6C, hnRNPA2B1 knockdown reduced *LNMAT2* levels only in the
15 exosomes secreted by BCa cells but had no effect on *LNMAT2* expression in BCa cells.
16 hnRNPA2B1 sorts RNAs into exosomes by recognizing a specific motif (i.e., GGAG) (29),
17 which is present on the hnRNPA2B1 binding sites (1930-1960 nt) of *LNMAT2*. Therefore, we
18 induced mutation at these sites and observed significantly decreased BCa cell production of
19 exosomal *LNMAT2*, indicating that the interaction between hnRNPA2B1 and these binding
20 sites is important for *LNMAT2* packaging into exosomes (Figure 7B and Supplemental Figure
21 6D). Additionally, in comparison with *miR-18a*, an miRNA retained in cells rather than
22 loaded into exosomes (29), *LNMAT2* presented a much higher exosome-to-cell ratio (Figure
23 7C and Supplemental Figure 6E), which is similar with the report by Villarroya-Beltri et al.,
24 who demonstrated hnRNPA2B1-mediated exosome packaging of *miR-198* (29). Moreover,
25 hnRNPA2B1 knockdown significantly decreased the enrichment of *LNMAT2* and *miR-198* in

1 BCa cell-secreted exosomes (Figure 7D and Supplemental Figure 6F), indicating that
2 *LNMAT2* is specifically sorted into exosomes in an hnRNPA2B1-dependent manner.

3 ***Exosomal LNMAT2 was internalized by HLECs to induce lymphangiogenesis***

4 As our results indicated that BCa cells-secreted exosomes promoted lymphangiogenesis,
5 we then evaluated the internalization of exosomes by HLECs. We labeled purified exosomes
6 with PKH67 green fluorescent dye and incubated them with HLECs for 12 h. Confocal
7 images showed the green fluorescent punctate signal in the cytoplasm of recipient HLECs,
8 indicating internalization of the PKH67-labeled exosomes, while no PKH67 fluorescent
9 signal was observed in the control group, suggesting that the HLECs internalized the BCa
10 cell-secreted exosomes (Figure 7E). We further examined whether exosomal *LNMAT2* was
11 successfully transferred into the HLECs and found that *LNMAT2* expression was significantly
12 increased in the HLECs after incubation with the exosomes (Figure 7F). Furthermore,
13 *LNMAT2* knockdown in 5637-EXO diminished their ability to induce *LNMAT2*
14 overexpression (Figure 7G), whereas UM-UC-3-EXO_{*LNMAT2*} increased *LNMAT2* expression
15 significantly in the HLECs (Supplemental Figure 7A).

16 To exclude the possibility that transcriptional activation of endogenous *LNMAT2* in the
17 HLECs activated the lymphangiogenesis, we established *LNMAT2*-knockout (KO) cells from
18 HLECs using the CRISPR-Cas9 approach with paired sgRNAs specifically targeting
19 *LNMAT2* (Supplemental Figure 7B). *LNMAT2* deficiency was subsequently detected in the
20 KO cells, suggesting successful inhibition of endogenous *LNMAT2* expression (Figure 7H).
21 We then evaluated the effects of exosomal *LNMAT2* on *LNMAT2*-wildtype (WT) and
22 *LNMAT2*-KO HLECs. Tube formation and Transwell assays both demonstrated that,
23 compared with exosomes secreted by si-NC-transfected 5637 cells (5637-EXO_{si-NC}),
24 exosomes secreted by si-*LNMAT2*#1-transfected 5637 cells (5637-EXO_{si-*LNMAT2*#1}) decreased
25 *LNMAT2*-KO HLEC proliferation and migration (Figure 7, I-K), while

1 UM-UC-3-EXO_{LNMAT2} had a promoting effect on *LNMAT2*-KO HLECs as compared with
2 UM-UC-3-EXO_{vector} (Supplemental Figure 7, C-E). These results were in accordance with
3 that for the *LNMAT2*-WT HLECs (Figure 7, I-K and Supplemental Figure 7, C-E). Taken
4 together, the results indicate that BCa cells induce lymphangiogenesis by transmitting
5 exosomal *LNMAT2* to HLECs.

6 ***Exosomal LNMAT2 upregulated PROX1 expression independently of VEGF-C***

7 Previously, we demonstrated that VEGF-C produced by tumor cells (3) and TAMs (4)
8 contributes to lymphangiogenesis and LN metastasis in BCa. However, >20% of BCa with
9 LN metastasis presents low VEGF-C expression (5). Our results showed that neither
10 *LNMAT2* overexpression nor *LNMAT2* knockdown in both 5637 and UM-UC-3 cells induced
11 VEGF-C mRNA or protein changes (Supplemental Figure 8, A-D), which suggested that
12 exosomal *LNMAT2*-induced lymphangiogenesis and LN metastasis in BCa might be through
13 a VEGF-C-independent mechanism.

14 It has been proposed that PROX1 is essential for lymphatic vascular system development
15 by regulating endothelial cell differentiation and metastatic dissemination (31, 32). ,
16 Interestingly, qRT-PCR and Western Blot analyses showed that PROX1 expression was
17 significantly increased in exosomal *LNMAT2*-treated HLECs as compared with the
18 control-treated HLECs (Figure 8, A and B and Supplemental Figure 8, E and F), indicating
19 that exosomal *LNMAT2* upregulated PROX1 expression in HLECs.

20 ***Exosomal LNMAT2 formed a DNA-RNA triplex with the PROX1 promoter***

21 To investigate the molecular mechanisms underlying exosomal *LNMAT2*-induced PROX1
22 expression in HLECs, we analyzed the subcellular location of exosomal *LNMAT2* after
23 internalization by *LNMAT2*-KO HLECs. Abundant *LNMAT2* was detected in the nucleus
24 (Supplemental Figure 8, G and H), indicating that *LNMAT2* released by BCa cell-secreted

1 exosomes translocated into the HLEC nucleus and exerted essential functions. Then, we
2 generated a series of luciferase constructs containing various lengths of the *PROX1* promoter
3 sequences, which is located from -2000 bp upstream to +200 bp downstream of the
4 transcriptional start site to explore whether exosomal *LNMAT2* transcriptionally upregulated
5 *PROX1*. Luciferase assays showed that the -650 to -350 bp region of *PROX1* promoter led to
6 an obvious increase of transcriptional activity in exosomal *LNMAT2*-induced HLECs (Figure
7 8C and Supplemental Figure 9A). Moreover, Chromatin isolation by RNA purification
8 (ChIRP) assays demonstrated that exosomal *LNMAT2* interacted physiologically with the P3
9 (-607 to -597 bp) region in the *PROX1* promoter in HLECs (Figure 8, D-F).

10 To further investigate whether *LNMAT2* directly interacted with *PROX1* promoter, we
11 obtained five potential pairs of triplex-forming oligonucleotides (TFOs) and their
12 corresponding triplex target sites (TTS) in the exosomal *LNMAT2* and *PROX1* promoter from
13 LongTarget (33), a tool for predicting lncRNA-DNA binding motifs, and each binding motif
14 was subjected to fluorescence resonance energy transfer (FRET) analysis and circular
15 dichroism (CD) spectroscopy (Supplemental Table 5). As shown in Figure 8G and
16 Supplemental Figure 9B, in comparison with the single-stranded RNA (ssRNA)/*PROX1* NC
17 group, the fluorescence signal was significantly increased at 570-580 nm and reduced at 520
18 nm in the *LNMAT2* (+2058 to +2069 nt)/*PROX1* TTS1 (-607 to -597 bp) group in FRET
19 analysis. These results was in accordance with the *FENDRR/PITX2* positive control group
20 (Supplemental Figure 9C) (34), indicating energy transfer from the fluorescein donor to the
21 rhodamine acceptor and supporting the formation of a triplex structure (4). CD spectroscopy
22 demonstrated a strong positive peak at 270-280 nm; a deep negative peak at 210 nm was
23 recorded in the *LNMAT2* (+2058 to +2069 nt)/*PROX1* TTS1 (-607 to -597 bp) group (Figure
24 8H and Supplemental Figure 9D), which was in accordance with the *FENDRR/PITX2*
25 positive control group (Supplemental Figure 9E). This validated the premise that the triplex

1 was constructed between *LNMAT2* and the *PROX1* promoter sequences in vitro. Additionally,
2 exosomal *LNMAT2* enhanced the luciferase intensity of the *PROX1* promoter, while no
3 obvious change was observed in the mutated *PROX1* promoter (*PROX1*-P3), suggesting that
4 the sequence between -607 and -597 bp in the *PROX1* promoter is of great significance for
5 exosomal *LNMAT2*-induced *PROX1* transactivation (Figure 8, I and J and Supplemental
6 Figure 9, F and G). Together, these data suggest that exosomal *LNMAT2* can form a triplex
7 with the lymphatic *PROX1* promoter sequence and upregulate its transcription levels.

8 ***Exosomal LNMAT2 interacted with hnRNPA2B1 to promote H3K4 trimethylation at the***
9 ***PROX1 promoter.***

10 hnRNPA2B1 is involved in H3K4 trimethylation (H3K4me3)-associated epigenetic
11 regulation by binding to the target DNA (35, 36). Accordingly, we explored whether
12 hnRNPA2B1 contributes to exosomal *LNMAT2*-induced transactivation of *PROX1* by
13 regulating H3K4me3 levels in the *PROX1* promoter region in HLECs. Chromatin
14 immunoprecipitation (ChIP) indicated enrichment of the *PROX1* promoter sequences
15 associated with hnRNPA2B1 and H3K4me3 in HLECs treated with exosomes secreted by
16 *LNMAT2*-transfected 5637 cells (5637-EXO_{*LNMAT2*}) and UM-UC-3-EXO_{*LNMAT2*} (Figure 8, K
17 and L and Supplemental Figure 9, H and I), whereas there was a significant reduction in
18 *PROX1* promoter sequences associated with hnRNPA2B1 and H3K4me3 in HLECs treated
19 with 5637-EXO_{si-*LNMAT2*#1} (Figure 8, M and N), suggesting that exosomal *LNMAT2*
20 upregulates *PROX1* expression by interacting directly with hnRNPA2B1 to increase
21 H3K4me3 levels in the *PROX1* promoter.

22 ***Exosomal LNMAT2-induced PROX1 upregulation promoted lymphatic metastasis***

23 Next, we clarified whether *PROX1* is required for exosomal *LNMAT2*-induced
24 lymphangiogenesis in BCa. Reducing *LNMAT2* expression in exosomes diminished tumor
25 induced HLEC proliferation and migration, ectopic *PROX1* rescued the effects (Figure 9,

1 A-C). In contrast, PROX1 silencing abolished exosomal *LNMAT2*-induced HLEC tube
2 formation and migration significantly and independently of VEGF-C (Supplemental Figure
3 10, A and B). These results suggested that PROX1 was required for exosomal
4 *LNMAT2*-mediated VEGF-C-independent lymphangiogenesis and lymphatic metastasis in
5 vitro. Furthermore, in vivo assays showed that the UM-UC-3-EXO_{*LNMAT2*} group exhibited
6 larger-volume popliteal LNs relative to the UM-UC-3-EXO_{vector} group after both had been
7 treated with VEGF-C-neutralizing antibody (pV1006R-r) (Figure 9, D-F).
8 Immunohistochemistry (IHC) of mouse BCa tissues also demonstrated that high *LNMAT2*
9 levels were accompanied by increased PROX1 expression in LYVE-1-positive lymphatic
10 vessels in both the intratumoral and peritumoral regions (Figure 9, G-I). The
11 UM-UC-3-EXO_{*LNMAT2*} group showed more enhancing effects on LN metastasis relative to the
12 UM-UC-3-EXO_{vector} group after pV1006R-r treatment in both, resulting in shorter survival
13 times (Figure 9, J and K and Supplemental Table 6). These results provide further evidence
14 that exosomal *LNMAT2* upregulates PROX1 expression to induce BCa lymphatic metastasis
15 in a VEGF-C-independent manner.

16 ***Exosomal LNMAT2 was associated with LN metastasis in BCa patients***

17 Accumulating evidence shows that BCa cell-secreted exosomal lncRNAs can be detected
18 in urine, and these urinary exosomal lncRNAs have been recognized as promising biomarkers
19 for early diagnosis of BCa (37). Therefore, clarifying the clinical significance of exosomal
20 *LNMAT2* in BCa LN metastasis would be of great significance. First, we found that *LNMAT2*
21 overexpression was associated with increased lymphatic vessel density in both the
22 intratumoral and peritumoral regions of BCa tissues in another 206-case cohort (Figure 10, A
23 and B). Interestingly, *LNMAT2* expression in urinary-EXO correlated positively with that in
24 paired tumor tissues (Supplemental Figure 11A). Consistently, ISH showed significantly
25 upregulated *LNMAT2* expression in tumor tissues from BCa patients with high exosomal

1 *LNMAT2* as compared with patients with low exosomal *LNMAT2* (Supplemental Figure 11, B
2 and C), implying that exosomal *LNMAT2* played a crucial role in *LNMAT2*-related LN
3 metastasis in BCa. Then, we explored whether exosomal *LNMAT2* was clinically relevant to
4 LN metastasis in BCa. Exosomal *LNMAT2* expression in BCa patients with LN metastasis
5 was dramatically higher than that in patients without LN metastasis (Figure 10C). Statistical
6 analysis revealed a positive correlation between exosomal *LNMAT2* and LN metastasis
7 (Supplemental Table 7). Moreover, Kaplan-Meier analysis showed that high exosomal
8 *LNMAT2* level was associated with poor prognosis of BCa (Figure 10, D and E). Univariate
9 and multivariate analysis also supported exosomal *LNMAT2* as an independent prognostic
10 factor of OS and DFS in BCa (Supplemental Table 8 and 9). Receiver operating characteristic
11 (ROC) analysis showed that urinary exosomal *LNMAT2* could discriminate between patients
12 with BCa and the healthy controls, and there was higher diagnostic accuracy, as measured by
13 the area under the curve (AUC), for diagnosing LN metastasis in BCa (Figure 10, F and G).
14 Consistently, we also found that exosomal *LNMAT2* was significantly elevated in BCa serum
15 samples and higher *LNMAT2* expression was detected in serum exosomes (serum-EXO) from
16 BCa patients with LN metastasis compared with that from patients without LN metastasis
17 (Supplemental Figure 11, D and E). Importantly, serum exosomal *LNMAT2* overexpression
18 correlated with shorter OS in BCa patients (Supplemental Figure 11F). Taken together, our
19 results suggest that exosomal *LNMAT2* might be a potential diagnostic biomarker and
20 therapeutic target for LN metastatic BCa.

1 **Discussion**

2 Lymphangiogenesis is the growth of new lymphatic vessels, which plays a crucial part in
3 LN metastasis (38). Although tumor-associated lymphangiogenesis is mainly driven by
4 VEGF-C, nearly 20% of BCa with LN metastasis show low VEGF-C expression (5, 6). So far,
5 the mechanism of lymphatic metastasis of BCa cells with low VEGF-C expression remains
6 unknown. Herein, we demonstrated that a tumor-secreted exosomal lncRNA is involved in
7 lymphangiogenesis and LN metastasis of BCa in a VEGF-C-independent manner. We
8 identified a novel lncRNA, *LNMAT2*, which is enriched in urinary exosomes and plays an
9 important role in BCa lymphatic metastasis. *LNMAT2* was packaged into exosomes via direct
10 interaction with hnRNPA2B1. Subsequently, exosomal *LNMAT2* was internalized by HLECs
11 and epigenetically activated PROX1 expression by recruiting hnRNPA2B1 to the *PROX1*
12 promoter, resulting in the lymphangiogenesis and lymphatic metastasis of BCa. These
13 findings provide in-depth mechanistic and translational insights into the pathway by which
14 exosomal lncRNA promotes BCa lymphatic metastasis in a VEGF-C-independent manner;
15 and that *LNMAT2* may emerge as a novel therapeutic target in BCa.

16 Exosomes have been extensively studied for their function in intercellular communication
17 between the tumor and the tumor microenvironment (TME) (12). Previously, several
18 independent studies have suggested that exosomal lncRNAs were involved in proliferation
19 (39), chemoresistance (40), and stemness (41) in various cancers. Herein, we found that
20 *LNMAT2* was overexpressed in urinary-EXO and serum-EXO from patients with BCa, and
21 both urinary and serum exosomal *LNMAT2* were positively associated with lymphatic
22 metastasis in patients with BCa, which indicated that exosomal RNA analysis could be
23 utilized for early detection of LN metastasis. Our results showed that exosomal *LNMAT2*
24 promoted lymphangiogenesis and LN metastasis of BCa, suggesting that *LNMAT2* may
25 represent a potential molecular target for clinical intervention in patients with BCa with LN

1 metastasis.

2 It is well-established that LN metastasis is a major cause of BCa-related mortality, and
3 intervention of LN metastasis might be a promising therapeutic strategy for improving the
4 prognosis of BCa (42, 43). Herein, a tumor-secreted exosomal *LNMAT2* emerged as a potent
5 target for diminishing lymphangiogenesis and LN metastasis in BCa, highlighting its
6 attractive role in cancer treatment. We demonstrated that downregulating exosomal *LNMAT2*
7 expression in BCa cells via RNA interference inhibited tumor-associated lymphangiogenesis
8 and might be a potential approach for suppressing LN metastasis. However, the stabilization
9 and delivery efficiency of siRNAs in vivo is one of the most critical issues in oligonucleotide
10 therapeutics. Locked nucleic acid (LNA) modification improved siRNA stability and
11 pharmacokinetics, and could be exploited to facilitate siRNA delivery into target cells,
12 resulting in effective suppression of tumor growth with minimal adverse effects in
13 experimental animal models (44). Therefore, inhibiting the function of exosomal *LNMAT2*
14 via LNA-modified siRNA might develop a new strategy for treating LN metastasis in human
15 cancer.

16 Exosomes regulate the biological functions of recipient cells via RNA transfer. The
17 exosomal RNAs are selectively sorted into exosomes by several RBPs (29, 30), including
18 hnRNPA2B1, which participates in exosomal RNA packaging by interacting with its target
19 RNAs (29). It has been demonstrated that hnRNPA2B1 regulates the localization of miRNA
20 into exosomes by binding to specific motifs (i.e., GGAG) (29). hnRNPA2B1 also plays a role
21 in loading a lncRNA (*IncARSR*) into exosomes (45). In the present study, we proposed a
22 model wherein hnRNPA2B1 binds specifically to *LNMAT2* through a specific sequence on
23 1930-1960 nt of *LNMAT2* and directs its packaging into exosomes. The identification of
24 hnRNPA2B1 for exporting *LNMAT2* in exosomes may provide unique strategies for
25 eliminating *LNMAT2* in the TME and for blocking exosomal *LNMAT2*-mediated BCa LN

1 metastasis.

2 Another important finding in the present study was that cancer-secreted exosomal
3 *LNMAT2* upregulated PROX1 expression epigenetically in HLECs. PROX1 is the key
4 transcription factor driving HLEC fate and specification by regulating the expression of
5 various lymphatic-specific proteins, including VEGFR3, LYVE-1, and podoplanin (9, 46).
6 PROX1 overexpression controls lymphangiogenesis by inducing HLEC proliferation and
7 migration (47, 48). Importantly, PROX1 depletion in mouse models causes lymphatic defects
8 that lead to mortality (9). Although several studies have indicated the essential role of
9 PROX1 in lymphangiogenesis, cancer induced *PROX1* transcription in HLECs remains
10 unknown. Herein, we demonstrated that BCa cell-secreted exosomal *LNMAT2* upregulated
11 PROX1 expression in HLECs by forming a DNA-RNA triplex with the binding site of the
12 *PROX1* promoter. PROX1 downregulation abolished the pro-lymphangiogenesis effect
13 induced by exosomal *LNMAT2*. Our findings uncovered a novel molecular mechanism
14 underlying the cancer-secreted exosomal lncRNA-mediated PROX1 overexpression in
15 HLECs, resulting in lymphangiogenesis and LN metastasis, which expanded current
16 knowledge on PROX1 regulation in HLECs.

17 In summary, our findings provided evidence of a VEGF-C-independent LN metastasis
18 mechanism in which BCa cell-secreted exosomal *LNMAT2* promoted lymphangiogenesis and
19 LN metastasis by transcriptionally upregulating *PROX1* in HLECs. We also found that
20 *LNMAT2* was overexpressed in both urinary-EXO and serum-EXO of BCa patients, which
21 positively correlated with both intratumoral and peritumoral lymphangiogenesis, and was
22 clinically relevant to BCa LN metastasis. Our study not only identifies a crucial mechanism
23 of exosomal lncRNA-mediated intercellular communication from BCa cells to the TME to
24 provoke LN metastasis, but also develops a potential non-invasive diagnostic approach and
25 therapeutic strategy for patients with BCa with LN metastasis.

1 **Methods**

2 *Clinical samples and study approval*

3 A total of 266 pairs of tumor tissues and NATs from patients with BCa who underwent
4 surgery was obtained at Sun Yat-sen Memorial Hospital (Cohort 1). Urine and blood samples
5 were obtained from another 206 patients with BCa and 120 healthy participants (Cohort 2). In
6 both cohorts, patients were eligible if they had pathologically confirmed BCa. The clinical
7 features of the patients are summarized in Supplemental Table 1 and Supplemental Table 7.
8 All experiments were conducted with the approval of the Committees for Ethical Review of
9 Research involving Human Subjects at Sun Yat-sen University. Informed consent was
10 obtained from all participants prior to sample collection.

11 *Cell lines and cell culture*

12 The human BCa cell lines UM-UC-3 (CRL-1749), 5637 (HTB-9), and T24 (HTB-4), and
13 the immortalized normal human urothelial cell line SV-HUC-1 (CRL-9520) were purchased
14 from American Type Culture Collection (VA, USA). UM-UC-3 and T24 cells were cultured
15 in DMEM (Gibco, NY, USA) supplemented with 10% FBS. The 5637 and SV-HUC-1 cells
16 were cultured in RPMI 1640 medium (Gibco, NY, USA) supplemented with 10% FBS and
17 F-12K medium (HyClone, UT, USA) supplemented with 10% FBS, respectively. HLECs
18 (#2500) were purchased from ScienCell Research Laboratories and cultured in endothelial
19 cell medium (ECM) (ScienCell Research Laboratories, CA, USA) supplemented with 5%
20 FBS. The cells were cultured in a humidified incubator with 5% CO₂ at 37°C.

21 *Mouse popliteal lymphatic metastasis model*

22 BALB/c nude mice (4-5 weeks old, 18-20g) were purchased from the Experimental
23 Animal Center, Sun Yat-sen University (Guangzhou, China) and were used for the lymphatic
24 metastasis model. All experimental procedures were conducted with the approval of the

1 Institutional Animal Care and Use Committee of Sun Yat-sen University. Luciferase-labeled
2 UM-UC-3 cells (5×10^6) were inoculated into the footpad of the mice. Then, the mice were
3 randomly divided into three groups ($n = 12$ or 16 per group) and injected intratumorally with:
4 (i) PBS, (ii) UM-UC-3-EXO_{Vector}, or (iii) UM-UC-3-EXO_{LNMAT2} (20 μ g per dose) every 3
5 days. Lymphatic metastasis was analyzed using a PerkinElmer IVIS Spectrum In Vivo
6 Imaging System. The footpad tumors and popliteal LNs were excised when the tumors were
7 200 mm³ (LN Volume (mm³) = (length[mm] \times width[mm]²) / 2). Serial sections of primary
8 tumors and popliteal LNs were analyzed by ISH and IHC. The sections were visualized with
9 a Nikon Eclipse Ti microscope. For survival analysis, the mice were observed until death or
10 were sacrificed by cervical dislocation 80 days after the first injection of PBS or exosomes.

11 ***RNA pull-down and RIP assays***

12 The *LNMAT2*-binding proteins were examined using RNA pull-down assays according to
13 the instructions of the PierceTM Magnetic RNA-Protein Pull-down Kit (Thermo Fisher
14 Scientific). Biotinylated *LNMAT2* and antisense sequences were synthesized using a
15 TranscriptAid T7 High Yield Transcription Kit (Thermo Fisher Scientific). The nuclear
16 fraction obtained using a NE-PER Nuclear Protein Extraction Kit (Thermo Fisher Scientific)
17 was incubated overnight with biotinylated *LNMAT2*, followed by precipitation with
18 streptavidin magnetic beads. The retrieved protein was eluted from the RNA-protein complex
19 and analyzed by immunoblotting or silver staining, followed by MS analysis with a
20 MALDI-TOF instrument (Bruker Daltonics).

21 The RIP assays were performed using an EZ-Magna RIP kit (Millipore). Lysates of 1×10^7
22 BCa cells obtained using complete RIP lysis buffer were immunoprecipitated with RIP buffer
23 containing anti-hnRNPA2B1 antibody-conjugated magnetic beads (Abcam, MA, USA). The
24 precipitated RNAs were analyzed by qRT-PCR. Mouse IgG and *UI* RNA were used as the
25 negative and non-specific control, respectively.

1 ***FRET and CD spectroscopy***

2 For FRET assays, 5-carboxytetramethylrhodamine (TAMRA)-labeled TFO and
3 5-carboxyfluorescein (FAM)-labeled TTS were generated and mixed in binding buffer (20
4 mM HEPES [pH 7.5], 10 mM MgCl₂, 50 mM sodium acetate) in a ratio of 1:5 (500 nM
5 TTS:2500 nM TFO). The mixtures were incubated at 55°C for 10 min, followed by 10 h
6 incubation at 37°C. The fluorescence wavelengths between 480 and 690 nm were measured
7 using a Molecular Device M5 Plate Reader.

8 For the CD spectroscopy, a 1:1 mixture of TFO (2.2 μM) and TTS oligos (2.2 μM) in
9 binding buffer (20 mM HEPES [pH 7.5], 10 mM MgCl₂, 50 mM sodium acetate) was
10 equilibrated at 30°C for 1 h. Control ssRNA/*PROX1* TTS and *FENDRR* TFO/*PITX2* TTS
11 were used as the negative and positive control, respectively. The measurements were
12 performed on a Chirascan spectrometer (Applied Photophysics). The oligos used in the FRET
13 and CD spectroscopy are listed in Supplemental Table 5.

14 ***Data availability***

15 The NGS data for this study (GSE106534, GSE106637) are available on the National
16 Center for Biotechnology Information website. All relevant data within the scope of the paper
17 are publicly available.

18 ***Bioinformatics analysis***

19 The hnRNPA2B1 binding motif enrichment in RNAs was obtained via POSTAR2. The
20 *LNMAT2* secondary structure was predicted using RNAalifold. The *LNMAT2* binding motifs
21 in the *PROX1* promoter and the binding sequences in *LNMAT2* were predicted by
22 LongTarget.

23 ***Statistics***

24 Statistical differences between groups were evaluated using SPSS v.13.0 (SPSS Inc.,

1 Chicago, IL, USA). Data were considered statistically significant if $P < 0.05$. All experiments
2 were performed in triplicate, and quantitative data are presented as the mean \pm SD. Statistical
3 significance for samples with non-normal distribution was identified using the
4 Mann-Whitney U test, two-tailed Student's t -test or one-way ANOVA was applied for
5 parametric variables, and the χ^2 test was applied for nonparametric variables. OS and DFS
6 were evaluated using the Kaplan-Meier method.

7 ***Study approval***

8 The use of human BCa tissue specimens was evaluated and approved by the Ethical
9 Committee of Sun Yat-sen Memorial Hospital, Sun Yat-sen University, and written informed
10 consent was obtained from all participants or their appropriate surrogates. All animal studies
11 were conducted with approval from the Sun Yat-sen University Institutional Animal Care and
12 Use Committee and were performed in accordance with established guidelines.

13

1 **Author contributions**

2 CC, JH, RC, and TL conceived, designed, and directed the study. YTL, YML, WH, and YZ
3 performed the in vitro and in vivo experiments and data analyses. YK, YZ and HL performed
4 the clinical data analyses. WH and GZ performed the ISH and IHC experiments. CC, JL, and
5 YML wrote and critically reviewed the manuscript. All authors read and approved the final
6 manuscript. Authorship order among the co-first authors was assigned based on their relative
7 contributions.

8 **Acknowledgments**

9 The authors thank Prof. JX Zhang of the Department of Medical Statistics and Epidemiology,
10 School of Public Health, Sun Yat-sen University, for statistical advice and research comments.
11 This study was funded by the National Key Research and Development Program of China
12 (Grant No. 2018YFA0902803); the National Natural Science Foundation of China (Grant No.
13 81825016, 81802530, 81830082, 81772719, 81772728, 91740119); Guangdong Medical
14 Research Foundation (Grant No. A2018330); Medical Scientific Research Foundation of
15 Guangdong Province (Grant No. A201947); Science and Technology Program of Guangzhou
16 (Grant No. 201604020156, 201604020177, 201707010116, 2017B020227007); National
17 Natural Science Foundation of Guangdong (Grant No. 2018A030313564, 2018A030310250,
18 2016A030313321); Yixian Youth project of Sun Yat-sen Memorial Hospital (Grant No.
19 YXQH201812); The Key Areas Research and Development Program of Guangdong (Grant
20 No. 2018B010109006); Guangdong Province Higher Vocational Colleges & Schools Pearl
21 River Scholar Funded Scheme (awarded to Tianxin Lin).

22

1 **Abbreviations**

2 BCa, bladder cancer; LN, lymph node; TAMs, tumor-associated macrophages; TME, tumor
3 microenvironment; HLECs, human lymphatic endothelial cells; lncRNA, long noncoding
4 RNA; *LNMAT2*, lymph node metastasis associated transcript 2; hnRNPA2B1, heterogeneous
5 nuclear ribonucleoprotein A2B1; PROX1, prospero homeobox 1; LYVE-1, lymphatic vessel
6 endothelial hyaluronan receptor 1; H3K4me3, H3K4 trimethylation; urinary-EXO, urinary
7 exosomes; NGS, next-generation sequencing; NAT, normal adjacent tissue; MIBC,
8 muscle-invasive bladder cancer; qRT-PCR, quantitative real-time PCR; TCGA, The Cancer
9 Genome Atlas; RACE, rapid amplification of cDNA ends; FISH, fluorescence in situ
10 hybridization; OS, overall survival; DFS, disease-free survival; ISH, in situ hybridization;
11 IHC, immunohistochemistry; 5637-EXO, exosomes secreted by 5637 cells; UM-UC-3-EXO,
12 exosomes secreted by UM-UC-3 cells; TEM, transmission electron microscopy; RIP, RNA
13 immunoprecipitation; KO, knockout; WT, wildtype; ChIRP, Chromatin isolation by RNA
14 purification; ChIP, Chromatin immunoprecipitation; FRET, fluorescence resonance energy
15 transfer; CD, circular dichroism; TFOs, triplex-forming oligonucleotides; TTS, triplex target
16 sites; UM-UC-3-EXO_{vector}, exosomes secreted by vector-transfected UM-UC-3 cells;
17 UM-UC-3-EXO_{LNMAT2}, exosomes secreted by *LNMAT2*-transfected UM-UC-3 cells;
18 5637-EXO_{si-LNMAT2}, exosomes secreted by si-*LNMAT2*-transfected 5637 cells; 5637-EXO_{si-NC},
19 exosomes secreted by si-NC-transfected 5637 cells; 5637-EXO_{vector}, exosomes secreted by
20 vector-transfected 5637 cells; 5637-EXO_{LNMAT2}, exosomes secreted by *LNMAT2*-transfected
21 5637 cells; ROC, receiver operating characteristic; AUC, area under the curve; serum-EXO,
22 serum exosomes; LNA, locked nucleic acid.

23

1

2 **References**

- 3 1. Bray F, Ferlay J, Soerjomataram I, Siegel RL, Torre LA, and Jemal A. Global cancer statistics 2018:
4 GLOBOCAN estimates of incidence and mortality worldwide for 36 cancers in 185 countries. *CA Cancer*
5 *J Clin.* 2018;68(6):394-424.
- 6 2. Hautmann RE, de Petriconi RC, Pfeiffer C, and Volkmer BG. Radical cystectomy for urothelial carcinoma
7 of the bladder without neoadjuvant or adjuvant therapy: long-term results in 1100 patients. *Eur Urol.*
8 2012;61(5):1039-47.
- 9 3. He W, Zhong G, Jiang N, Wang B, Fan X, Chen C, et al. Long noncoding RNA BLACAT2 promotes bladder
10 cancer-associated lymphangiogenesis and lymphatic metastasis. *J Clin Invest.* 2018;128(2):861-75.
- 11 4. Chen C, He W, Huang J, Wang B, Li H, Cai Q, et al. LNMAT1 promotes lymphatic metastasis of bladder
12 cancer via CCL2 dependent macrophage recruitment. *Nat Commun.* 2018;9(1):3826.
- 13 5. Zu X, Tang Z, Li Y, Gao N, Ding J, and Qi L. Vascular endothelial growth factor-C expression in bladder
14 transitional cell cancer and its relationship to lymph node metastasis. *BJU Int.* 2006;98(5):1090-3.
- 15 6. Suzuki K, Morita T, and Tokue A. Vascular endothelial growth factor-C (VEGF-C) expression predicts
16 lymph node metastasis of transitional cell carcinoma of the bladder. *Int J Urol.* 2005;12(2):152-8.
- 17 7. Saharinen P, Tammela T, Karkkainen MJ, and Alitalo K. Lymphatic vasculature: development, molecular
18 regulation and role in tumor metastasis and inflammation. *Trends Immunol.* 2004;25(7):387-95.
- 19 8. Plate K. From angiogenesis to lymphangiogenesis. *Nat Med.* 2001;7(2):151-2.
- 20 9. Wigle JT, Harvey N, Detmar M, Lagutina I, Grosveld G, Gunn MD, et al. An essential role for Prox1 in
21 the induction of the lymphatic endothelial cell phenotype. *EMBO J.* 2002;21(7):1505-13.
- 22 10. Flister MJ, Wilber A, Hall KL, Iwata C, Miyazono K, Nisato RE, et al. Inflammation induces
23 lymphangiogenesis through up-regulation of VEGFR-3 mediated by NF-kappaB and Prox1. *Blood.*
24 2010;115(2):418-29.
- 25 11. Zhang ZG, Buller B, and Chopp M. Exosomes - beyond stem cells for restorative therapy in stroke and
26 neurological injury. *Nat Rev Neurol.* 2019;15(4):193-203.
- 27 12. Xu R, Rai A, Chen M, Suwakulsiri W, Greening DW, and Simpson RJ. Extracellular vesicles in cancer -
28 implications for future improvements in cancer care. *Nat Rev Clin Oncol.* 2018;15(10):617-38.
- 29 13. Fang JH, Zhang ZJ, Shang LR, Luo YW, Lin YF, Yuan Y, et al. Hepatoma cell-secreted exosomal
30 microRNA-103 increases vascular permeability and promotes metastasis by targeting junction proteins.
31 *Hepatology.* 2018;68(4):1459-75.
- 32 14. Pan Y, Hui X, Hoo RLC, Ye D, Chan CYC, Feng T, et al. Adipocyte-secreted exosomal microRNA-34a
33 inhibits M2 macrophage polarization to promote obesity-induced adipose inflammation. *J Clin Invest.*
34 2019;129(2):834-49.
- 35 15. Cheng M, Yang J, Zhao X, Zhang E, Zeng Q, Yu Y, et al. Circulating myocardial microRNAs from infarcted
36 hearts are carried in exosomes and mobilise bone marrow progenitor cells. *Nat Commun.*
37 2019;10(1):959.
- 38 16. Zhang H, Deng T, Liu R, Bai M, Zhou L, Wang X, et al. Exosome-delivered EGFR regulates liver
39 microenvironment to promote gastric cancer liver metastasis. *Nat Commun.* 2017;8:15016.
- 40 17. Zeng Z, Li Y, Pan Y, Lan X, Song F, Sun J, et al. Cancer-derived exosomal miR-25-3p promotes
41 pre-metastatic niche formation by inducing vascular permeability and angiogenesis. *Nat Commun.*
42 2018;9(1):5395.
- 43 18. Fang T, Lv H, Lv G, Li T, Wang C, Han Q, et al. Tumor-derived exosomal miR-1247-3p induces
44 cancer-associated fibroblast activation to foster lung metastasis of liver cancer. *Nat Commun.*

- 1 2018;9(1):191.
- 2 19. Mathieu M, Martin-Jaular L, Lavieu G, and Thery C. Specificities of secretion and uptake of exosomes
3 and other extracellular vesicles for cell-to-cell communication. *Nat Cell Biol.* 2019;21(1):9-17.
- 4 20. Ji H, Cao R, Yang Y, Zhang Y, Iwamoto H, Lim S, et al. TNFR1 mediates TNF-alpha-induced tumour
5 lymphangiogenesis and metastasis by modulating VEGF-C-VEGFR3 signalling. *Nat Commun.*
6 2014;5:4944.
- 7 21. Chen F, Chen J, Yang L, Liu J, Zhang X, Zhang Y, et al. Extracellular vesicle-packaged
8 HIF-1alpha-stabilizing lncRNA from tumour-associated macrophages regulates aerobic glycolysis of
9 breast cancer cells. *Nat Cell Biol.* 2019;21(4):498-510.
- 10 22. Karaman S, and Detmar M. Mechanisms of lymphatic metastasis. *J Clin Invest.* 2014;124(3):922-8.
- 11 23. Seok Y, Yang HC, Kim TJ, Lee KW, Kim K, Jheon S, et al. Frequency of lymph node metastasis according
12 to the size of tumors in resected pulmonary adenocarcinoma with a size of 30 mm or smaller. *J Thorac*
13 *Oncol.* 2014;9(6):818-24.
- 14 24. Liu YY, Fang WL, Wang F, Hsu JT, Tsai CY, Liu KH, et al. Does a Higher Cutoff Value of Lymph Node
15 Retrieval Substantially Improve Survival in Patients With Advanced Gastric Cancer?-Time to Embrace a
16 New Digit. *Oncologist.* 2017;22(1):97-106.
- 17 25. Rault-Petit B, Do Cao C, Guyétant S, Guimbaud R, Rohmer V, Julié C, et al. Current Management and
18 Predictive Factors of Lymph Node Metastasis of Appendix Neuroendocrine Tumors: A National Study
19 From the French Group of Endocrine Tumors (GTE). *Ann Surg.* 2019;270(1):165-171.
- 20 26. Moran-Jones K, Wayman L, Kennedy DD, Reddel RR, Sara S, Snee MJ, et al. hnRNP A2, a potential
21 ssDNA/RNA molecular adapter at the telomere. *Nucleic Acids Res.* 2005;33(2):486-96.
- 22 27. Zhu Y, Xu G, Yang YT, Xu Z, Chen X, Shi B, et al. POSTAR2: deciphering the post-transcriptional
23 regulatory logics. *Nucleic Acids Res.* 2019;47(D1):D203-D11.
- 24 28. Hu B, Yang YT, Huang Y, Zhu Y, and Lu ZJ. POSTAR: a platform for exploring post-transcriptional
25 regulation coordinated by RNA-binding proteins. *Nucleic Acids Res.* 2017;45(D1):D104-D14.
- 26 29. Villarroya-Beltri C, Gutierrez-Vazquez C, Sanchez-Cabo F, Perez-Hernandez D, Vazquez J,
27 Martin-Cofreces N, et al. Sumoylated hnRNP2B1 controls the sorting of miRNAs into exosomes
28 through binding to specific motifs. *Nat Commun.* 2013;4:2980.
- 29 30. Shurtleff MJ, Temoche-Diaz MM, Karfilis KV, Ri S, and Schekman R. Y-box protein 1 is required to sort
30 microRNAs into exosomes in cells and in a cell-free reaction. *Elife.* 2016;5.pii:e19276.
- 31 31. Park KJ, Cho SB, Park YL, Kim N, Park SY, Myung DS, et al. Prospero homeobox 1 mediates the
32 progression of gastric cancer by inducing tumor cell proliferation and lymphangiogenesis. *Gastric*
33 *Cancer.* 2017;20(1):104-15.
- 34 32. Cho H, Kim J, Ahn JH, Hong YK, Makinen T, Lim DS, et al. YAP and TAZ Negatively Regulate Prox1 During
35 Developmental and Pathologic Lymphangiogenesis. *Circ Res.* 2019;124(2):225-42.
- 36 33. He S, Zhang H, Liu H, and Zhu H. LongTarget: a tool to predict lncRNA DNA-binding motifs and binding
37 sites via Hoogsteen base-pairing analysis. *Bioinformatics.* 2015;31(2):178-86.
- 38 34. Grote P, and Herrmann BG. The long non-coding RNA Fendrr links epigenetic control mechanisms to
39 gene regulatory networks in mammalian embryogenesis. *RNA Biol.* 2013;10(10):1579-85.
- 40 35. Tchurikov NA, Fedoseeva DM, Sosin DV, Snezhkina AV, Melnikova NV, Kudryavtseva AV, et al. Hot spots
41 of DNA double-strand breaks and genomic contacts of human rDNA units are involved in epigenetic
42 regulation. *J Mol Cell Biol.* 2015;7(4):366-82.
- 43 36. Tchurikov NA, Kretova OV, Fedoseeva DM, Sosin DV, Grachev SA, Serebraykova MV, et al. DNA
44 double-strand breaks coupled with PARP1 and HNRNPA2B1 binding sites flank coordinately expressed

- 1 domains in human chromosomes. *PLoS Genet.* 2013;9(4):e1003429.
- 2 37. Zhan Y, Du L, Wang L, Jiang X, Zhang S, Li J, et al. Expression signatures of exosomal long non-coding
3 RNAs in urine serve as novel non-invasive biomarkers for diagnosis and recurrence prediction of
4 bladder cancer. *Mol Cancer.* 2018;17(1):142.
- 5 38. Alitalo K, Tammela T, and Petrova TV. Lymphangiogenesis in development and human disease. *Nature.*
6 2005;438(7070):946-53.
- 7 39. Xue M, Chen W, Xiang A, Wang R, Chen H, Pan J, et al. Hypoxic exosomes facilitate bladder tumor
8 growth and development through transferring long non-coding RNA-UCA1. *Mol Cancer.*
9 2017;16(1):143.
- 10 40. Xu H, Han H, Song S, Yi N, Qian C, Qiu Y, et al. Exosome-Transmitted PSMA3 and PSMA3-AS1 Promote
11 Proteasome Inhibitor Resistance in Multiple Myeloma. *Clin Cancer Res.* 2019;25(6):1923-35.
- 12 41. Ren J, Ding L, Zhang D, Shi G, Xu Q, Shen S, et al. Carcinoma-associated fibroblasts promote the
13 stemness and chemoresistance of colorectal cancer by transferring exosomal lncRNA H19.
14 *Theranostics.* 2018;8(14):3932-48.
- 15 42. Fernandez MI, Bolenz C, Trojan L, Steidler A, Weiss C, Alken P, et al. Prognostic implications of
16 lymphangiogenesis in muscle-invasive transitional cell carcinoma of the bladder. *Eur Urol.*
17 2008;53(3):571-8.
- 18 43. Kluth LA, Black PC, Bochner BH, Catto J, Lerner SP, Stenzl A, et al. Prognostic and Prediction Tools in
19 Bladder Cancer: A Comprehensive Review of the Literature. *Eur Urol.* 2015;68(2):238-53.
- 20 44. Fluiter K, Mook OR, and Baas F. The therapeutic potential of LNA-modified siRNAs: reduction of
21 off-target effects by chemical modification of the siRNA sequence. *Methods Mol Biol.*
22 2009;487:189-203.
- 23 45. Qu L, Ding J, Chen C, Wu ZJ, Liu B, Gao Y, et al. Exosome-Transmitted lncARSR Promotes Sunitinib
24 Resistance in Renal Cancer by Acting as a Competing Endogenous RNA. *Cancer Cell.*
25 2016;29(5):653-68.
- 26 46. Lee S, Kang J, Yoo J, Ganesan SK, Cook SC, Aguilar B, et al. Prox1 physically and functionally interacts
27 with COUP-TFII to specify lymphatic endothelial cell fate. *Blood.* 2009;113(8):1856-9.
- 28 47. Cha B, Geng X, Mahamud MR, Zhang JY, Chen L, Kim W, et al. Complementary Wnt Sources Regulate
29 Lymphatic Vascular Development via PROX1-Dependent Wnt/beta-Catenin Signaling. *Cell Rep.*
30 2018;25(3):571-84 e5.
- 31 48. Wong BW, Wang X, Zecchin A, Thienpont B, Cornelissen I, Kalucka J, et al. The role of fatty acid
32 beta-oxidation in lymphangiogenesis. *Nature.* 2017;542(7639):49-54.
- 33

34

Figure 1

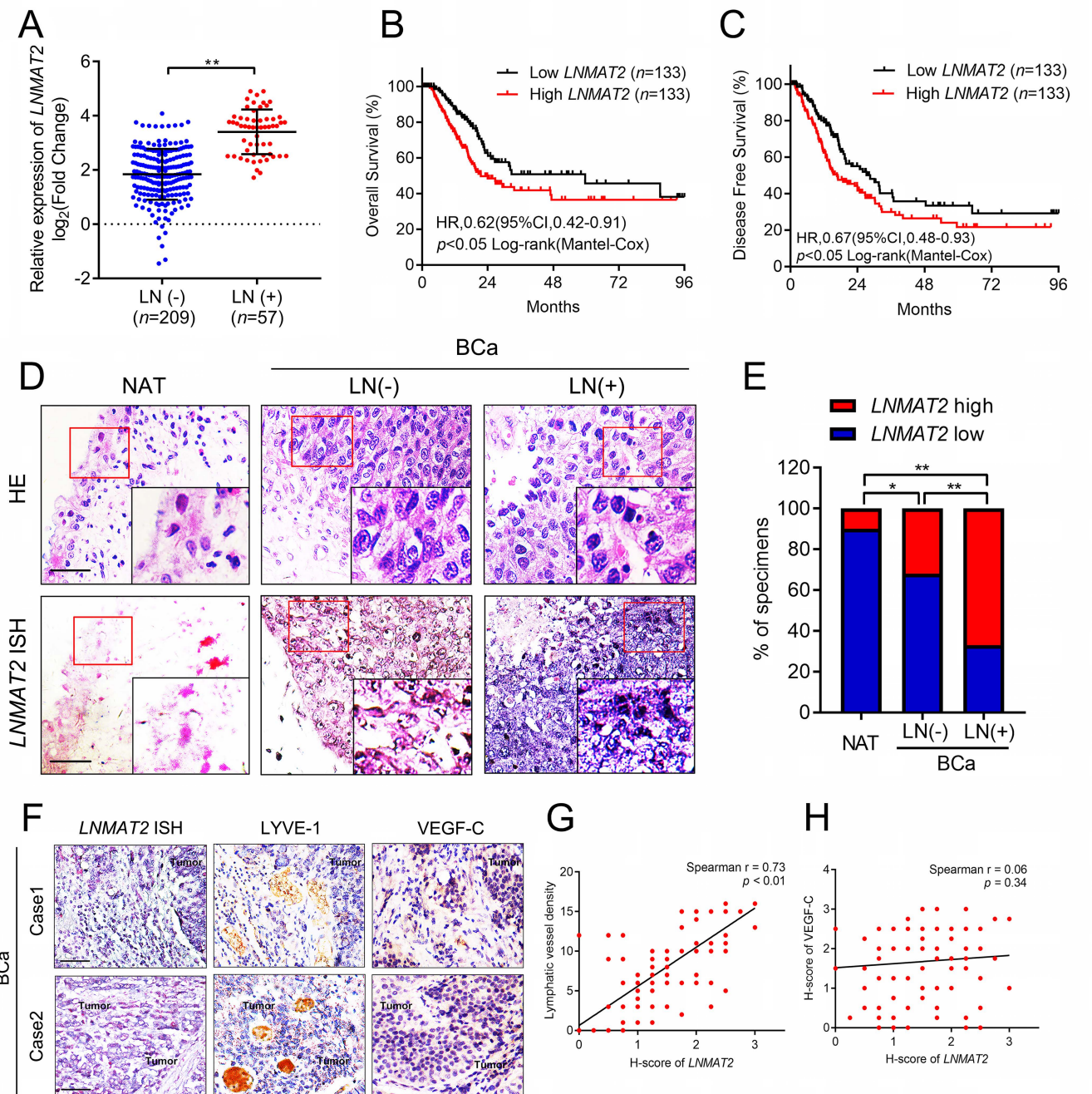


Figure 1. *LNMT2* overexpression is associated with BCa lymphatic metastasis. (A) qRT-PCR analysis of *LNMT2* expression in a cohort of 266 BCa patients according to LN status. Groups were compared using the nonparametric Mann-Whitney *U* test. *GAPDH* was used as an internal control. (B and C) The OS (B) and DFS (C) of patients with BCa with lower vs. higher *LNMT2* expression were estimated using Kaplan-Meier curves. The median expression was used as the cut-off value. (D and E) Representative ISH images (D) and percentages (E) of *LNMT2* expression (blue) in paraffin-embedded NAT and BCa tissue with or without LN metastasis ($n = 266$). Scale bars: 50 μm . Statistical significance was assessed by χ^2 test. (F-H) Representative images (F) and correlation analysis (G and H) of ISH and IHC staining showing positive correlation between *LNMT2* expression and lymphatic vessel density indicated by anti-LYVE-1 staining, and that *LNMT2* expression was not correlated with VEGF-C levels in the BCa tissues ($n = 266$). Scale bars: 50 μm . * $P < 0.05$, ** $P < 0.01$.

Figure 2

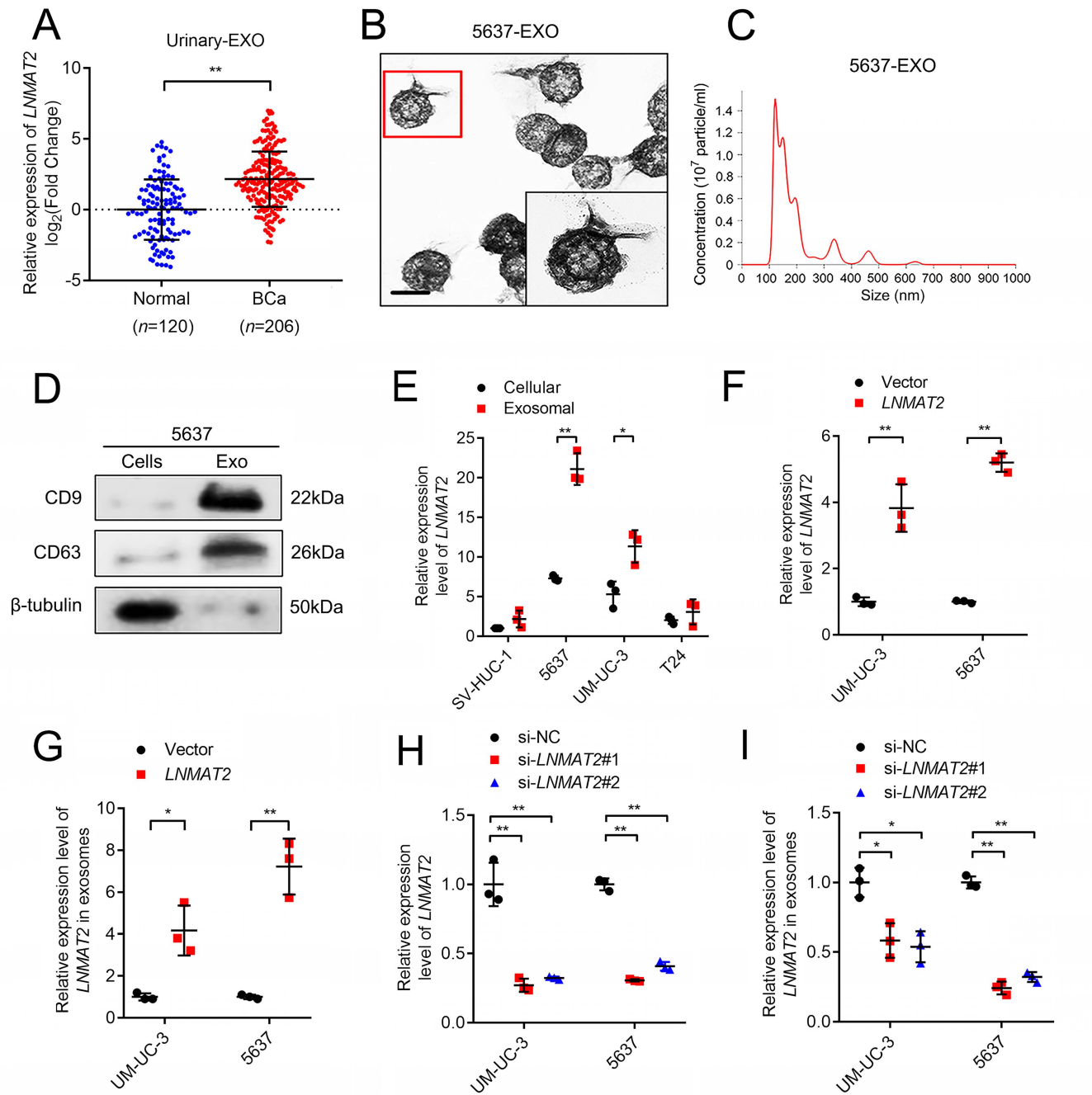


Figure 2. *LNMAT2* is upregulated in BCa cells-secreted exosomes. (A) qRT-PCR analysis of *LNMAT2* expression in urinary-EXO from 206 patients with BCa and 120 healthy participants. *GAPDH* was used as an internal control. Groups were compared using the nonparametric Mann-Whitney *U* test. (B and C) Purified 5637-EXO were identified by TEM (B) and NanoSight (C). Scale bar: 100 nm. (D) Western Blot analysis of exosomal protein markers in 5637 cell lysates or 5637-EXO. (E) qRT-PCR analysis of *LNMAT2* expression levels in bladder cell lines and in their corresponding exosomes. *GAPDH* was used as an internal control. Statistical significance was assessed using one-way ANOVA followed by Dunnett's tests. (F and G) qRT-PCR analysis of *LNMAT2* expression in *LNMAT2*-overexpressing, control BCa cells (F), and their corresponding exosomes (G). *GAPDH* was used as an internal control. Statistical significance was assessed using two-tailed Student's *t*-test followed by Dunnett's tests for multiple comparisons. (H and I) qRT-PCR analysis of *LNMAT2* expression in *LNMAT2* knockdown, control BCa cells (H), and their corresponding exosomes (I). *GAPDH* was used as an internal control. Statistical significance was assessed using one-way ANOVA followed by Dunnett's tests for multiple comparisons. Error bars represent the SD of three independent experiments. **P* < 0.05, ***P* < 0.01.

Figure 3

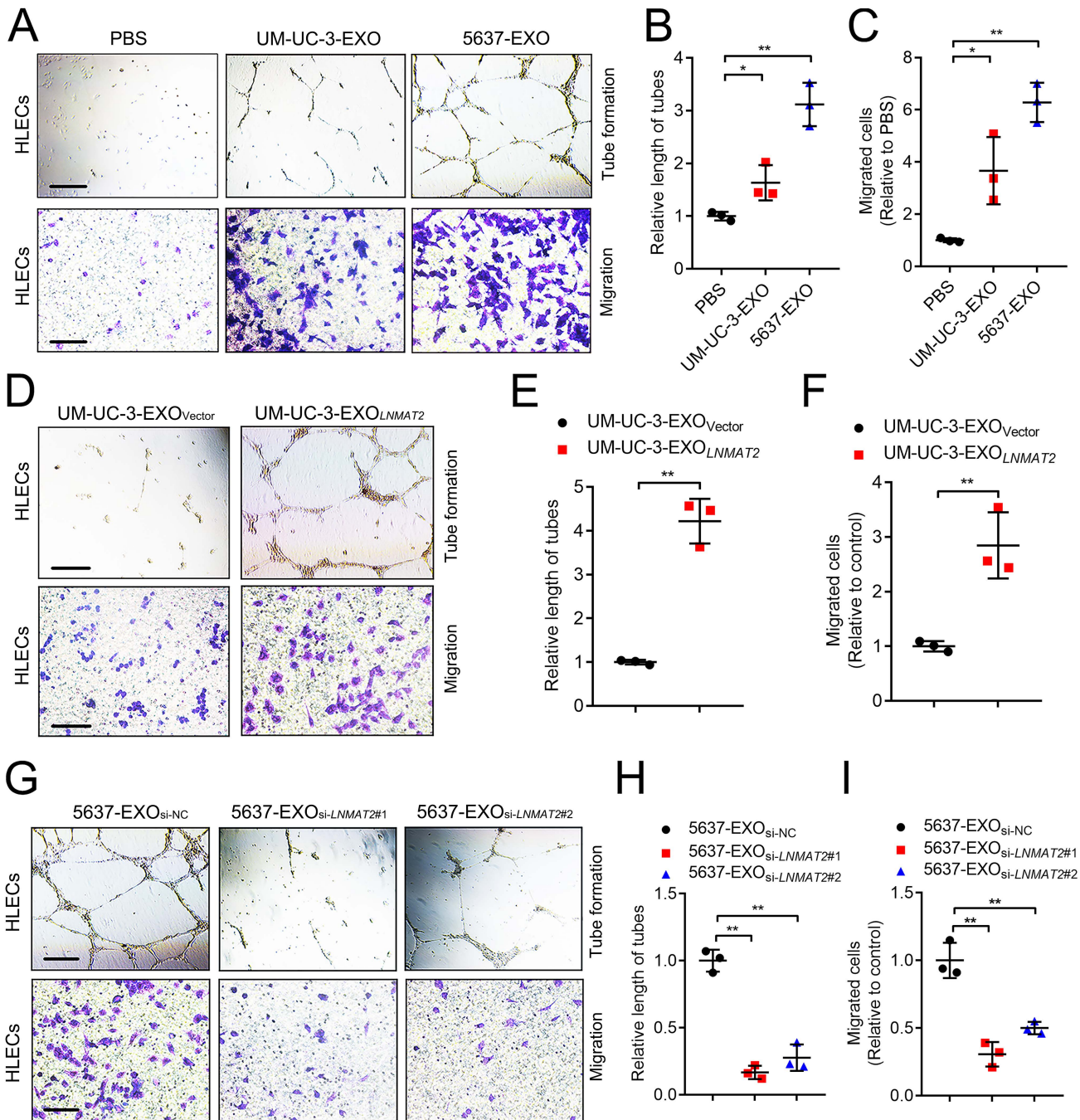


Figure 3. Exosomal *LNMAT2* promotes lymphangiogenesis in vitro. (A-C) Representative images (A) and quantification of tube formation (B) and Transwell migration (C) by HLECs treated with PBS, 5637-EXO, or UM-UC-3-EXO. Scale bars: 100 μ m. Statistical significance was assessed using one-way ANOVA followed by Dunnett's tests. (D-F) Representative images (D) and quantification of tube formation (E) and Transwell migration (F) by HLECs treated with UM-UC-3-EXO_{Vector} or UM-UC-3-EXO_{LNMAT2}. Scale bars: 100 μ m. Statistical significance was assessed using two-tailed Student's *t*-test. (G-I) Representative images (G) and quantification of tube formation (H) and Transwell migration (I) by HLECs treated with 5637-EXO_{si-NC}, 5637-EXO_{si-LNMAT2#1}, or 5637-EXO_{si-LNMAT2#2}. Scale bars: 100 μ m. Statistical significance was assessed using one-way ANOVA followed by Dunnett's tests. Error bars represent the SD of three independent experiments. * $P < 0.05$, ** $P < 0.01$.

Figure 4

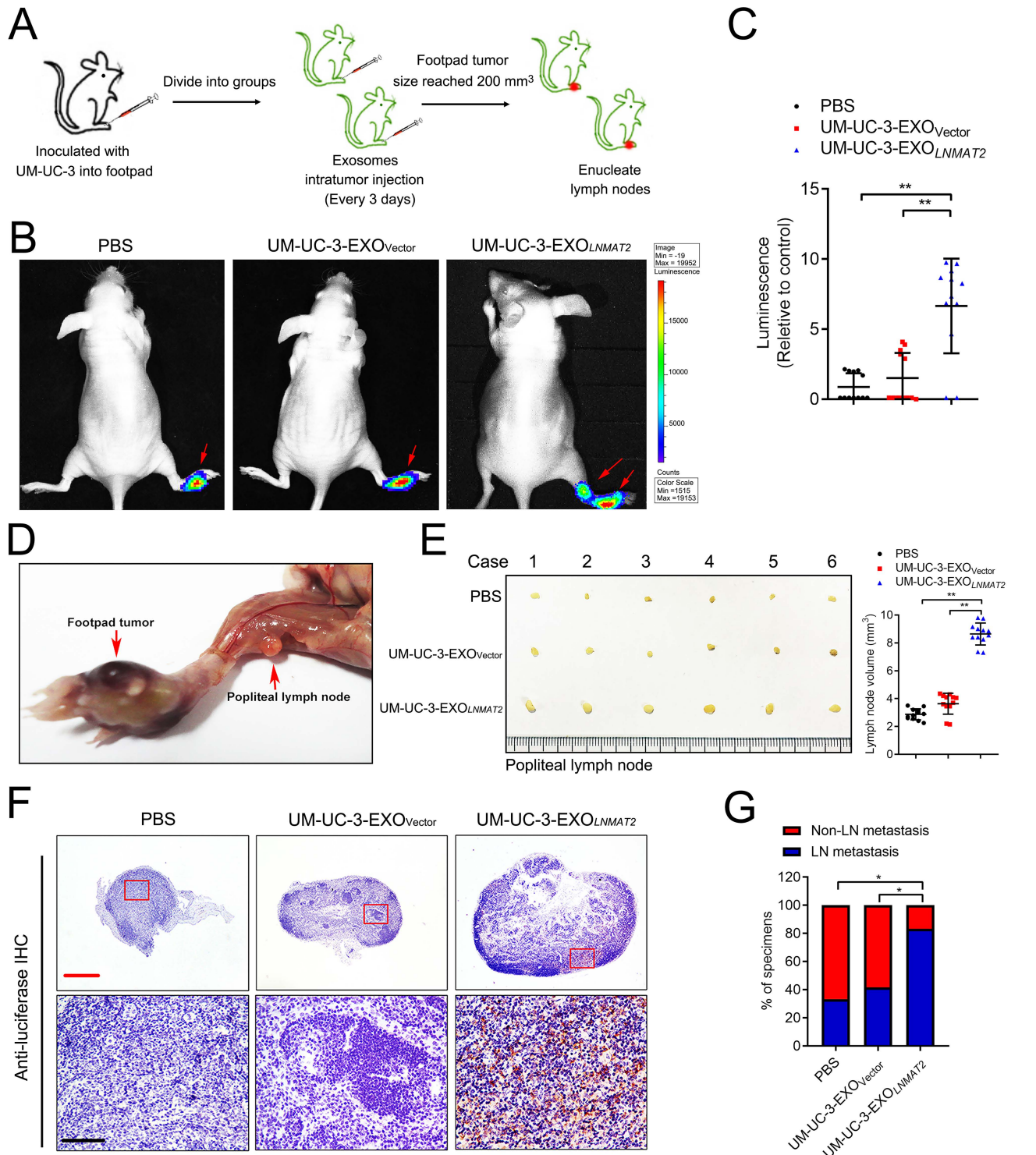


Figure 4. Exosomal *LNMAT2* promotes lymphatic metastasis in vivo. (A) Schematic representation of establishment of the nude mouse model of popliteal LN metastasis. (B and C) Representative bioluminescence images (B) and histogram analysis (C) of popliteal metastatic LN from nude mice treated with PBS, UM-UC-3-EXO_{vector}, or UM-UC-3-EXO_{LNMAT2} after UM-UC-3 cells had been inoculated into the footpad ($n = 12$). Red arrow indicates footpad tumor and metastatic popliteal LN. Statistical significance was assessed using one-way ANOVA followed by Dunnett's tests. (D) Representative image of the popliteal LN metastasis model. (E) Representative images of enucleated popliteal LNs (left) and histogram analysis (right) of the LN volume of all groups ($n = 12$). Statistical significance was assessed using one-way ANOVA followed by Dunnett's tests. (F) Representative images of IHC staining with anti-luciferase antibody ($n = 12$). Scale bars: 500 μ m (red) or 50 μ m (black). (G) The percentages of LN status in all groups ($n = 12$). Statistical significance was assessed by χ^2 test. Error bars represent the SD of three independent experiments. * $P < 0.05$, ** $P < 0.01$.

Figure 5

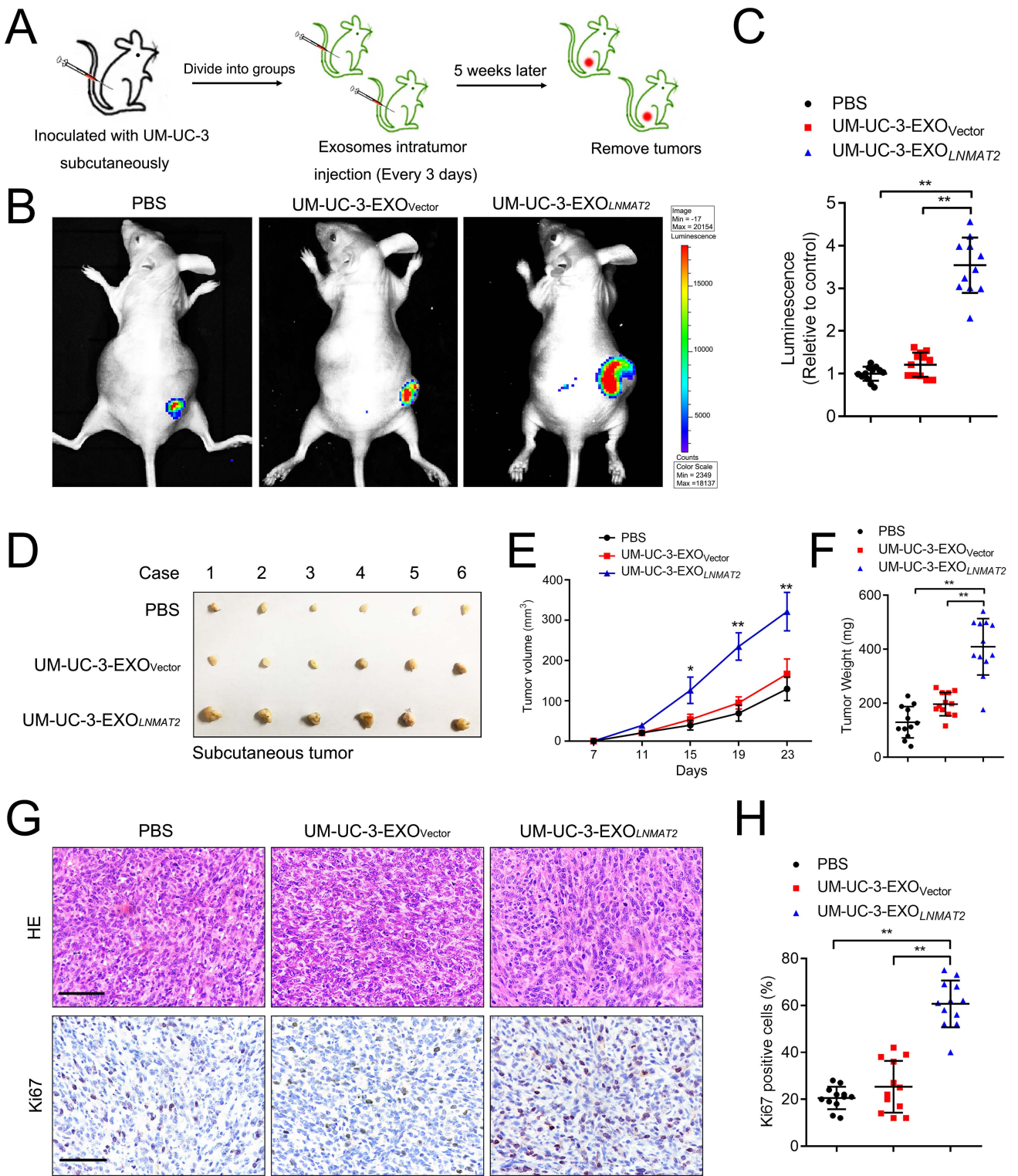


Figure 5. Exosomal *LNMAT2* promotes BCa tumorigenesis in vivo. (A) Schematic representation of the establishment of the xenograft model. (B and C) Representative bioluminescence images (B) and histogram analysis (C) of subcutaneous tumors from nude mice treated with PBS, UM-UC-3-EXO_{Vector}, or UM-UC-3-EXO_{LNMAT2} ($n = 12$). Statistical significance was assessed using one-way ANOVA followed by Dunnett's tests. (D) Representative images of gross appearance of subcutaneous tumors from nude mice treated with PBS, UM-UC-3-EXO_{Vector}, or UM-UC-3-EXO_{LNMAT2} ($n = 12$). (E and F) The measured tumor volumes (E) and weights (F) ($n = 12$). Statistical significance was assessed using one-way ANOVA followed by Dunnett's tests. (G and H) Representative images (G) and histogram analysis (H) of IHC staining for Ki-67 expression ($n = 12$). Scale bars: 50 μm . Statistical significance was assessed using one-way ANOVA followed by Dunnett's tests. Error bars represent the SD of three independent experiments. * $P < 0.05$, ** $P < 0.01$.

Figure 6

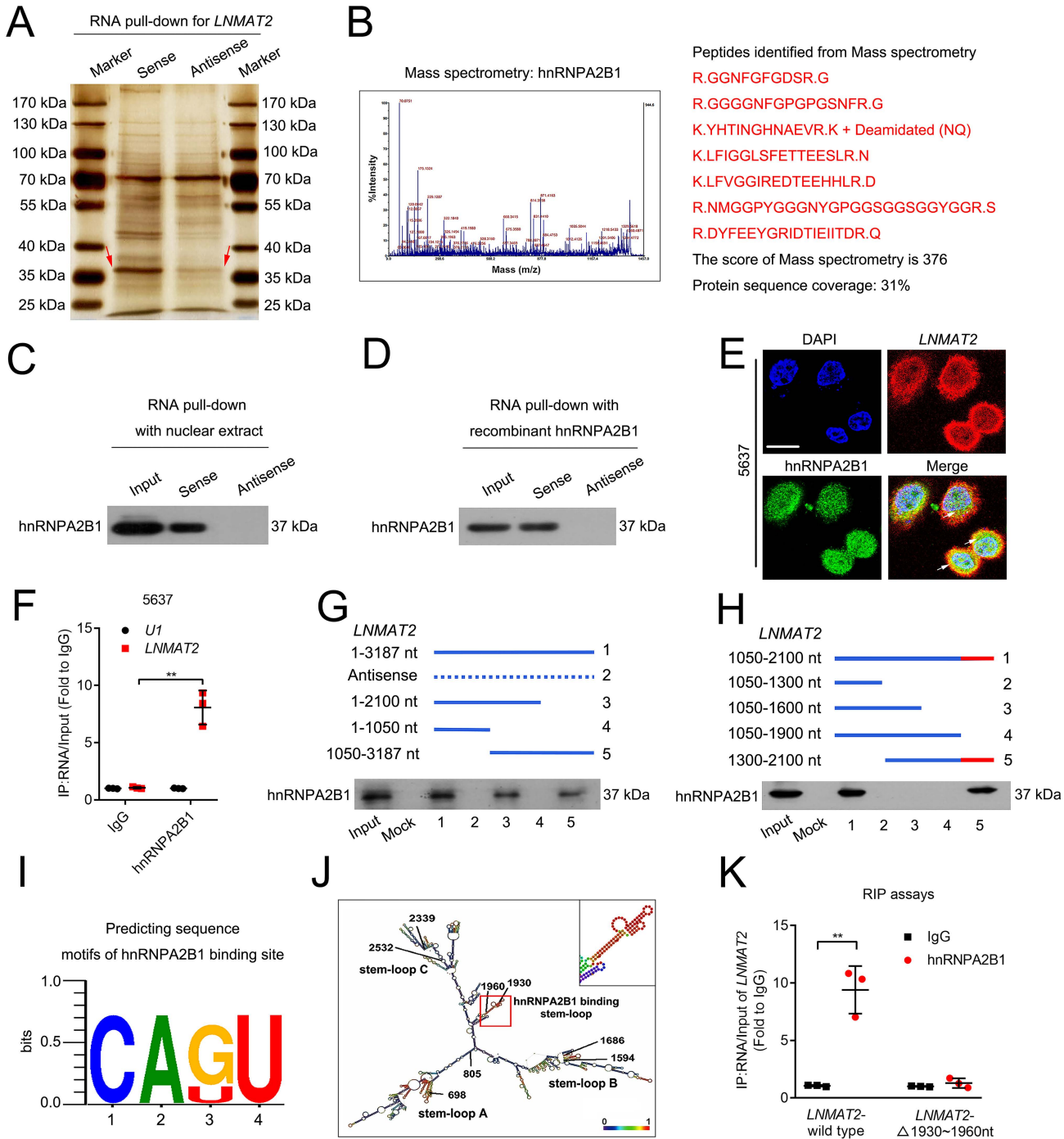


Figure 6. Direct interaction of *LNMAT2* with hnRNP A2B1. (A) RNA pull-down assay using *LNMAT2* sense and antisense RNAs in 5637 cells, followed by silver staining. Red arrows indicate hnRNP A2B1. (B) MS identification of *LNMAT2*-binding proteins. (C and D) RNA pull-down and Western Blot with 5637 cell nuclear extract (C) or purified recombinant hnRNP A2B1 (D) confirmed that *LNMAT2* was associated with hnRNP A2B1. (E) Fluorescence assessment of *LNMAT2* and hnRNP A2B1 colocalization in 5637 cells. Scale bars: 5 μ m. (F) RIP analysis using the anti-hnRNP A2B1 antibody revealing that *LNMAT2* interacted with hnRNP A2B1 in 5637 cells. Negative control, IgG; non-specific control, *U1*. Statistical significance was assessed using two-tailed Student's *t* test. (G and H) Serial deletions of *LNMAT2* were used in RNA pull-down assays to identify regions required for *LNMAT2* and hnRNP A2B1 interaction. (I) POSTAR2 prediction of sequence motifs of hnRNP A2B1 binding sites. (J) RNAalifold predicted that *LNMAT2* would have four stable stem-loop structures. The inset (framed in red) indicates the hnRNP A2B1 binding stem-loop structures in *LNMAT2*. (K) RIP assays performed after site-directed mutagenesis of 1930-1960 nt of *LNMAT2* in 5637 cells. Statistical significance was assessed using two-tailed Student's *t*-test. Error bars represent the SD of three independent experiments. **P* < 0.05, ***P* < 0.01.

Figure 7

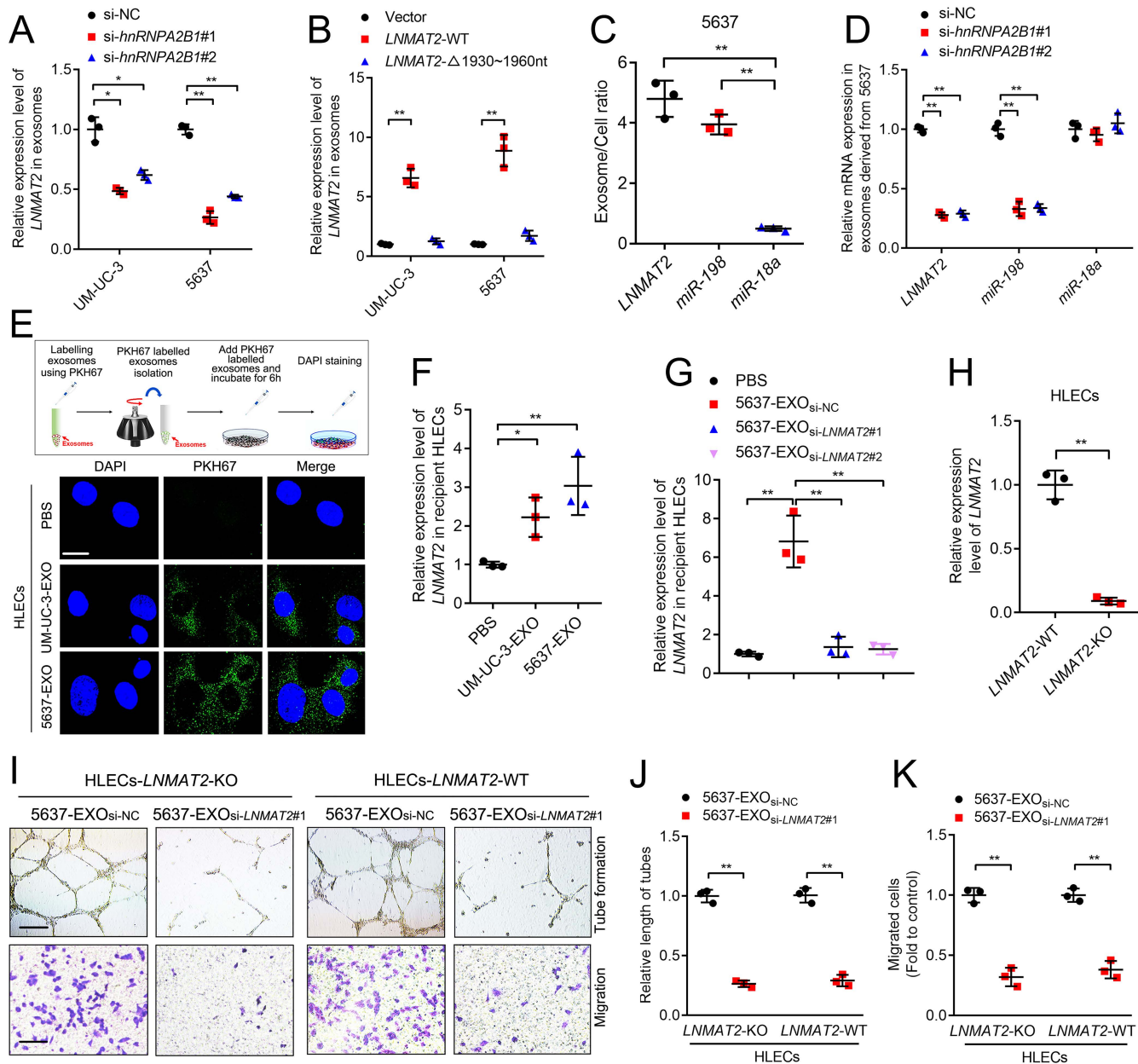


Figure 7. *LNMAT2* is packaged into exosomes in an *hnRNPA2B1*-dependent manner and transported to HLECs. (A) qRT-PCR analysis of *LNMAT2* expression in exosomes secreted by *hnRNPA2B1* knockdown cells. Statistical significance was assessed using one-way ANOVA followed by Dunnett's tests. (B) qRT-PCR analysis of *LNMAT2* expression in BCa cell-secreted exosomes. Statistical significance was assessed using one-way ANOVA followed by Dunnett's tests. (C) The exosome:cell ratio of RNAs in 5637 cells obtained by qRT-PCR. Statistical significance was assessed using one-way ANOVA followed by Dunnett's tests. (D) qRT-PCR analysis of RNA levels in exosomes secreted by *hnRNPA2B1* knockdown 5637 cells. Statistical significance was assessed using one-way ANOVA followed by Dunnett's tests. (E) Schematic illustration of exosome internalization assays and representative images of HLEC fluorescence after incubation with PKH67-labeled (green) BCa cell exosomes. Scale bar: 5 μ m. (F and G) qRT-PCR analysis of *LNMAT2* expression in HLECs treated with PBS, 5637-EXO, UM-UC-3-EXO (F) or 5637-EXO_{si-NC}, 5637-EXO_{si-*LNMAT2*#1}, or 5637-EXO_{si-*LNMAT2*#2} (G). Statistical significance was assessed using one-way ANOVA followed by Dunnett's tests for multiple comparisons. (H) qRT-PCR confirming the *LNMAT2* knockout. Statistical significance was assessed using two-tailed Student's *t*-test. (I-K) Representative images (I) and quantification of tube formation (J) and Transwell migration (K) by HLECs (*LNMAT2*-KO or *LNMAT2*-WT) after treating with 5637-EXO_{si-NC} or 5637-EXO_{si-*LNMAT2*#1}. Scale bars: 100 μ m. Statistical significance was assessed using two-tailed Student's *t*-test. *GAPDH* was used as an internal control for qRT-PCR analysis in Figure A-H. Error bars represent the SD of three independent experiments. **P* < 0.05, ***P* < 0.01.

Figure 8

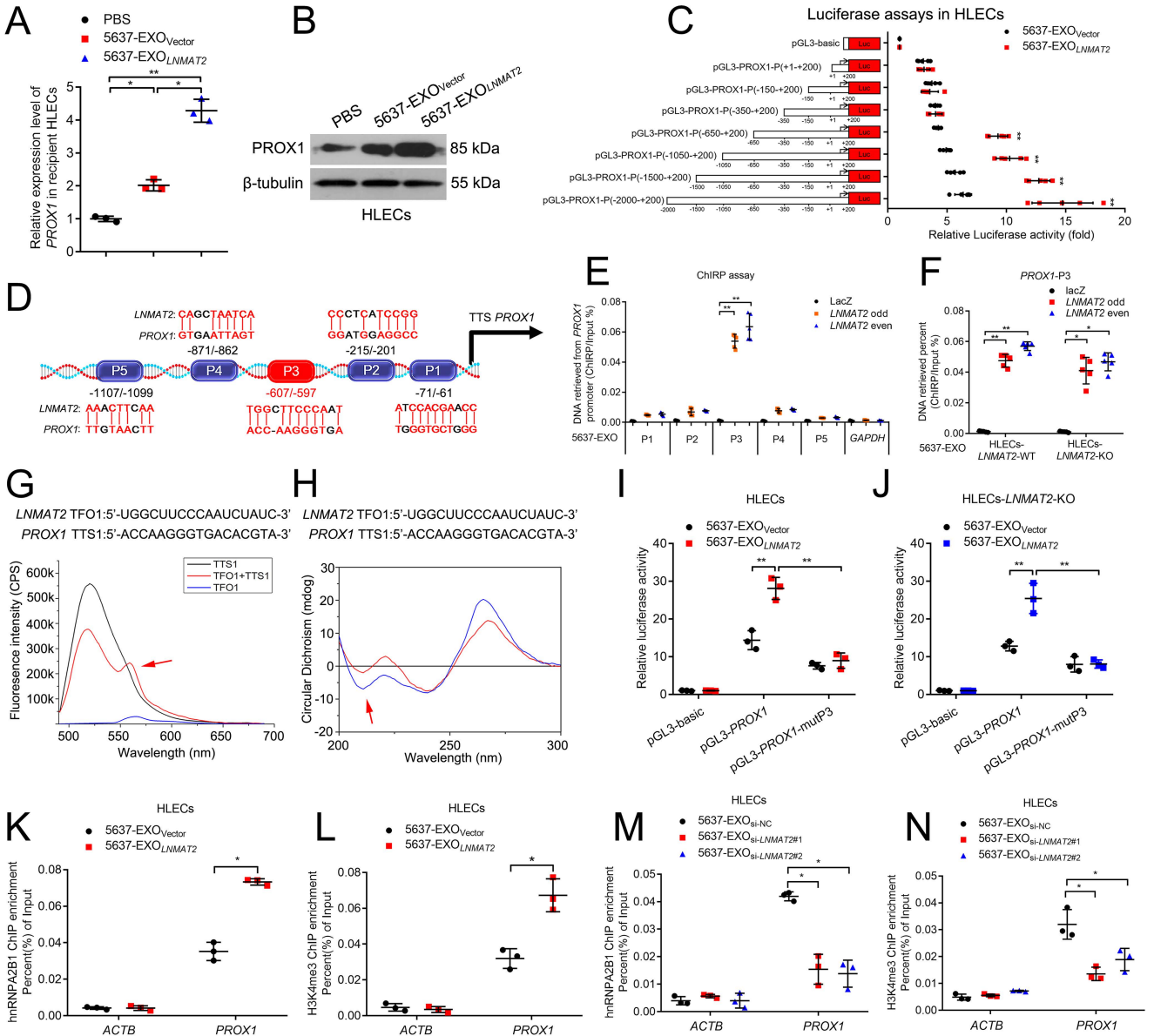


Figure 8. Exosomal *LNMAT2* forms a DNA-RNA triplex with the *PROX1* promoter. (A and B) qRT-PCR (A) and Western Blot (B) of *PROX1* expression in HLECs treated with PBS, 5637-EXO_{Vector}, or 5637-EXO_{LNMAT2}. *GAPDH* was used as an internal control in qRT-PCR. Statistical significance was assessed using one-way ANOVA followed by Dunnett's tests. (C) Sequential deletions for evaluating the transcriptional activity of the *PROX1* promoter in HLECs treated with 5637-EXO_{Vector} or 5637-EXO_{LNMAT2}. Statistical significance was assessed using one-way ANOVA followed by Dunnett's tests. (D) Schematic presentation of the predicted *LNMAT2* binding sites in the *PROX1* promoter. (E) ChIRP of *LNMAT2*-associated chromatin in HLECs treated with 5637-EXO. Statistical significance was assessed using two-tailed Student's *t*-test. (F) ChIRP of *LNMAT2*-associated chromatin in *LNMAT2*-WT or *LNMAT2*-KO HLECs treated with 5637-EXO. Statistical significance was assessed using two-tailed Student's *t*-test. (G) FRET of a 1:5 mixture (red) of TFO (black) in *LNMAT2* with TTS (blue) in the *PROX1* promoter. (H) CD spectrum of a 1:1 mixture of TFO in *LNMAT2* with TTS in the *PROX1* promoter (red). The sum of the TFO and TTS is shown in blue. (I and J) Evaluation of WT or *LNMAT2* binding site mutated *PROX1* promoter in *LNMAT2*-WT (I) or *LNMAT2*-KO (J) HLECs, respectively, treated with 5637-EXO_{Vector} or 5637-EXO_{LNMAT2}. Statistical significance was assessed using one-way ANOVA followed by Dunnett's tests. (K-N) ChIP-qPCR of hnRNP A2B1 occupancy (K and M) and H3K4me3 (L and N) status in the *PROX1* promoter after HLEC incubation with indicated exosomes. Statistical significance was assessed using two-tailed Student's *t*-test and one-way ANOVA followed by Dunnett's tests for multiple comparisons. Error bars represent the SD of three independent experiments. **P* < 0.05, ***P* < 0.01.

Figure 9

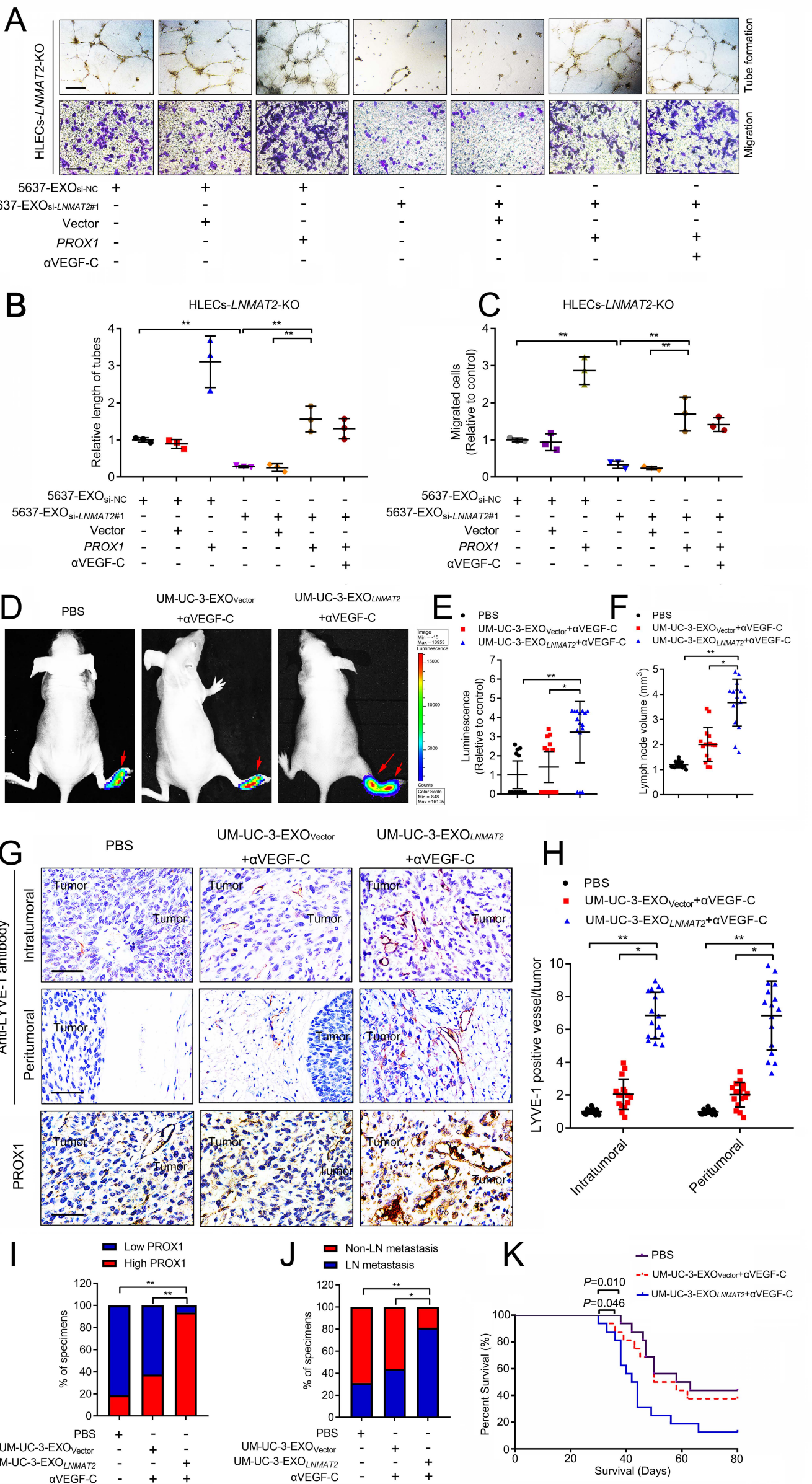


Figure 10

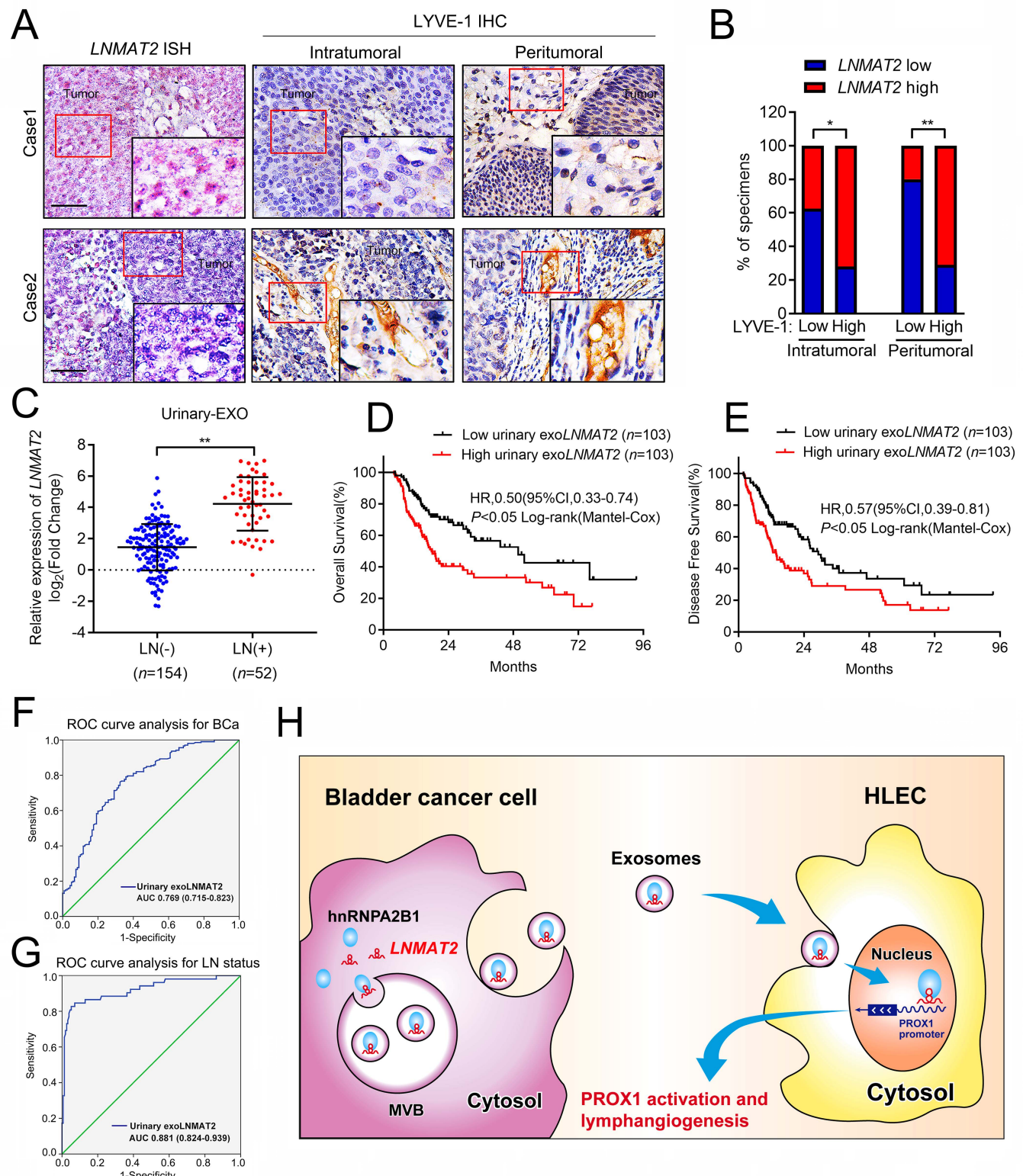


Figure 10. Exosomal LNMAT2 is associated with BCa lymphatic metastasis. (A and B) Representative images (A) and percentages (B) of BCa tissues ($n = 206$) with high and low LYVE-1 levels in the intratumoral and peritumoral lymphatic vessels in patients with different expression of LNMAT2. Scale bars: 50 μm . Statistical significance was assessed by χ^2 test. **(C)** qRT-PCR analysis of LNMAT2 expression in a 206-patient cohort of urinary-EXO from BCa patients with or without LN metastasis. GAPDH was used as an internal control. Groups were compared using the Nonparametric Mann-Whitney U test. **(D and E)** Kaplan-Meier curves of OS (D) and DFS (E) of patients with BCa according to the relative urinary exosomal LNMAT2 expression. The median expression was used as the cut-off value ($n = 206$). **(F and G)** ROC curve analyses for evaluating the diagnostic potential of urinary exosomal LNMAT2 for BCa (F) and LN metastasis (G). **(H)** Proposed model of BCa cell-secreted exosomal LNMAT2-mediated PROX1 activation in HLECs for promoting lymphangiogenesis and LN metastasis. * $P < 0.05$, ** $P < 0.01$.